J. Fluid Mech. (1998), *vol.* 365, *pp.* 137–170. Printed in the United Kingdom

© 1998 Cambridge University Press

Stability of a dusty-gas laminar boundary layer on a flat plate

By EVGENY S. ASMOLOV
AND SERGEI V. MANUILOVICH

Zhukovsky Central Aero-Hydrodynamics Institute, Zhukovsky, Moscow region, 140160, Russia
e-mail: aes@aerocentr.msk.su

(Received 11 July 1996 and in revised form 8 October 1997)

The linear stability of incompressible boundary-layer flow of dusty gas on a semi-infinite flat plate is considered. The particles are assumed to be under the action of the Stokes drag only. The problem is reduced to the solution of the modified Orr–Sommerfeld equation (Saffman 1962). This is solved numerically using two approaches: directly by orthonormalization method, and by perturbation method at small particle mass content. The stability characteristics are calculated for both mono- and polydisperse particles.

The dust suppresses the instability waves for a wide range of the particle size. The most efficient suppression takes place when the relaxation length of the particle velocity is close to the wavelength of the Tollmien–Schlicting (TS) wave. The reduction in growth rate per unit dust content is approximately ten times greater than the characteristic value of the growth rate for a clean gas.

For monosized dust the complex frequency of the TS wave changes in a discontinuous way. As a result a domain in the space of independent parameters arises where two discrete TS modes exist and a domain where no TS mode may exist. For polydisperse dust with a discrete distribution in particle size the number of breaks in the dependence equals the number of particle sizes. For the continuous distribution in particle size the dependence of the complex-frequency on Reynolds number and wavenumber is continuous. The eigenfunction becomes a non-smooth function of the normal coordinate in this case.

Some comments are made about the role of the lift force acting on the particles for the problem in question.

1. Introduction

Laminar–turbulent transition in shear fluid flows is the subject of considerable discussion; however, it has not yet received much attention for a fluid containing small particles. For a concentrated suspension the particle influence on the stability of two-phase flow is due to the change of the physical properties of the medium (effective density and viscosity). The stability characteristics in this case are still determined from the solution of the Orr–Sommerfeld equation. This type of stability problem was considered for sedimentation flows inside an inclined settler (Shaqfeh & Acrivos 1987) and for Poiseuille resuspension flow (Zhang, Acrivos & Schaflinger 1992).

When the particulate volume fraction is low, the particle–fluid interaction is due to viscous drag force. As a result the particles may influence both steady mean flow

https://doi.org/10.1017/S0022112098001256 Published online by Cambridge University Press

and the unsteady perturbations. Particle motion under the action of Stokes drag is characterized by the time and length scales (Marble 1962; Saffman 1962)

$$\tau_{St}^{\circ} = \frac{2}{9}\frac{a^{\circ 2}}{\nu^{\circ}}\frac{\rho_p^{\circ}}{\rho^{\circ}}, \qquad L_{St}^{\circ} = \tau_{St}^{\circ} U_{\infty}^{\circ} \tag{1.1}$$

of particle velocity relaxation. Hereinafter superscript $\circ$ denotes dimensional values: a° is the particle radius, ν° is the kinematic viscosity of the gas, ρ_p° and ρ° are the densities of the particle material and the gas, U_{∞}° is the characteristic velocity of the flow. The unsteady slip velocity is finite when the relaxation length is of order of or greater than the characteristic wavelength of the instability wave L_{TS}°. For the opposite case of fine dust, $L_{St}^{\circ} \ll L_{TS}^{\circ}$, the slip velocity is small.

Linearized Navier–Stokes equations for a plane parallel flow of incompressible fluid, accounting for the momentum transfer between phases, and the momentum equations for homogeneously distributed particles have been reduced to a single ordinary differential equation (Saffman 1962). It differs from the ordinary Orr–Sommerfeld equation for a clean gas in that the mean-flow velocity is replaced by a modified velocity profile which is a complex function of the space coordinate. It contains three dimensionless parameters: one characterizing the gas flow, the Reynolds number R, and two for the dust, namely the mass concentration of the particles f and the relaxation time introduced by

$$S = \tau_{St}^{\circ}\nu^{\circ}/L_{TS}^{\circ 2}. \tag{1.2}$$

Two limiting cases of fine and coarse dust were considered. When $RS \ll 1$, both the mean-flow and the perturbed velocities of the particles resemble closely those of the gas. Thus fine dust makes the flow similar to that of a clean gas with the same mean-flow profile but with a density being equal to $1 + f$. As a result the effective Reynolds number of the basic flow increases, and the dust effect is destabilizing. In the opposite limiting case of coarse dust, when $RS \gg 1$, the particles do not move with the gas when the flow is perturbed but have the velocity of the mean flow. They dissipate the energy of disturbances and stabilize the flow.

A single attempt to solve the modified Orr–Sommerfeld equation numerically was made by Michael (1964) for plane Poiseuille flow of dusty gas by means of the perturbation method. The displacement of the neutral stability curve with respect to the clean-gas position was calculated using approximate interpolations of the eigenfunction and adjoint function of the Orr–Sommerfeld equation for a clean gas. Calculations show the significant growth of the critical Reynolds number even at low ($f = 0.05$) particle concentration. However, at $RS > 20$ the calculated data are questionable since the position of the neutral stability curve varies in an irregular way. The main features of the modified Orr–Sommerfeld equation have not been investigated properly yet. It has a singular point if the space variable y is considered as a complex one. The reason for the inadequacy of the results at large S, apparently, is that the numerical technique did not take into account the strong variation of the integrand for the case when the singular point is close to the real y-axis.

The stability of multiphase mixing-layer flow was investigated by Yang *et al.* (1990). A modified Rayleigh equation was solved numerically. It was shown that the particles enhance the stability of two-phase flow and reduce the growth rate of perturbations.

In all papers cited where the modified Orr–Sommerfeld or Rayleigh equations were considered only the unsteady momentum transfer between phases was taken into account. This is valid, and the mean-flow velocity distribution $U(y)$ is the same as for a particle-free flow, for example, for plane Poiseuille flow. In this case the equations

https://doi.org/10.1017/S0022112098001256 Published online by Cambridge University Press

governing the mean flow do not contain the density. However, $U(y)$ for the dusty-gas mixing layer or for the boundary-layer flow, considered in present paper, will differ from those for a clean gas.

The main object of the present paper is to calculate the characteristics of the Tollmien–Schlicting (TS) wave for the boundary-layer flow of dusty gas over a semi-infinite flat plate. Both monosized and polydisperse particles are considered. The preliminary results were presented in IUTAM Symposia on laminar–turbulent transition (Asmolov & Manuilovich 1994, 1995).

The relaxation length of the particle velocity, L°_{St}, is assumed to be small compared with the characteristic distance from the leading edge of the plate, X°, and of the order of the characteristic wavelength of the TS wave, L°_{TS}. Under these assumptions the small-slip regime (Marble 1962, 1970) for the mean boundary-layer flow occurs. This steady dusty-gas flow behaves like a clean-gas flow with density equal to the net upstream density of two phases. The velocity field can be expressed in terms of the classical Blasius solution.

When the particles' mass fraction is low, they only slightly affect the fluid mean flow. However, their influence on the instability wave may be significant in this case. In the unsteady perturbed velocity field the particles cannot accommodate rapid acceleration but tend to slip through the gas because $L^\circ_{TS} \sim L^\circ_{St}$. The unsteady drag force acts on the disperse phase, and an equal but opposite volume force acts on the gas. For this reason a small portion of the disperse phase can suppress the instability wave.

To describe the perturbed flow the quasi-parallel approach (Lin 1955) is used. Then the linearized equations for the perturbations are reduced to the modified Orr–Sommerfeld equation. Its eigenvalues and eigenfunctions are evaluated using the direct numerical integration method and the perturbation theory. The first can be used for arbitrary particle mass content but the second only at small f.

The dust suppresses the instability wave for a wide range of the particle size. Efficient damping takes place when L°_{St} is near to L°_{TS}. In this case the reduction in growth rate per unit dust content is approximately ten times greater than the characteristic value of the growth rate for a clean gas.

For dusty gas containing monosized particles the singular point results in a discontinuity in the complex frequency ω of the TS wave. As a result there is a domain in a space of independent parameters where two discrete TS mode exist, and a domain where no TS mode may exist. For polydisperse dust having a continuous distribution in particle size the complex frequency depends on Reynolds number and wavenumber continuously, but the eigenfunction becomes non-smooth.

The effect of the lift force on the particles which is due to the combination of the slip and the shear is also discussed.

2. Governing equation

Consider the linear stability problem for a boundary-layer flow of incompressible gas containing particles of the same radius a°. We introduce a coordinate system, with the origin at some point on the plate surface, with a streamwise x-axis and with the y-axis normal to it (see figure 1). The particle phase has a uniform upstream volume concentration N_∞.

The problem is studied under the usual assumptions of the dusty-gas flow approach (Marble 1962; Saffman 1962). The volume fraction of the particles is infinitesimally small, so that the interactions between them can be neglected. However, the mass

https://doi.org/10.1017/S0022112098001256 Published online by Cambridge University Press

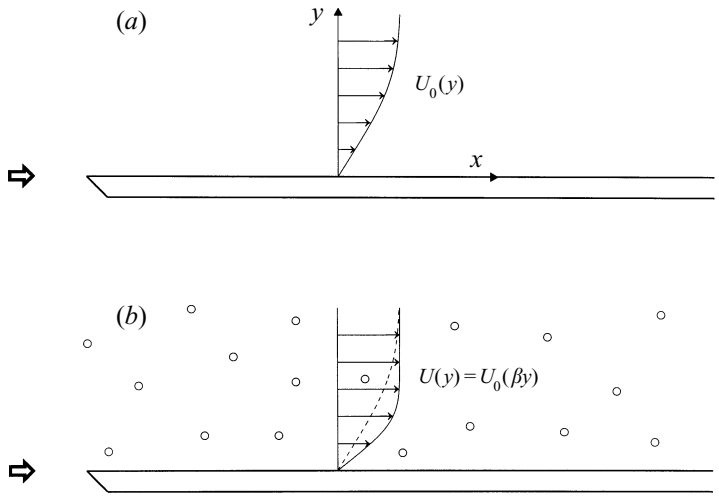


FIGURE 1. Configuration of the flow. Boundary layer of (*a*) a clean and (*b*) dusty gas.

content of the dust may be finite, since the density of the particle material is much greater than that of the gas. The particle velocity and density are described by continuum fields. The effect of the dust on the gas is equivalent to an extra force per unit volume. The particle Reynolds number based on the slip velocity is small, so that the Stokes drag law for this force can be used. The effect of the lift force on the particles which is due to the combination of the slip and the shear is neglected. The extent to which the last assumption is valid is considered in § 8.

The two-dimensional fields of the gas velocity and pressure, and the dust velocity and volume density are presented in the form of the superposition of the steady flow and small unsteady perturbations of the mean flow respectively as

$$U_x^\circ + \epsilon u_x^\circ, \quad U_y^\circ + \epsilon u_y^\circ, \quad P^\circ + \epsilon p^\circ,$$

$$V_x^\circ + \epsilon v_x^\circ, \quad V_y^\circ + \epsilon v_y^\circ, \quad N + \epsilon n,$$

where $\epsilon \ll 1$ is the amplitude of the perturbations.

The relaxation length of the particle velocity due to Stokes drag, L_{St}°, is assumed to be small compared with the distance X° between the leading edge of the plate and the coordinate origin. The steady flow of a dusty gas in a laminar boundary layer over a flat plate for this limiting case (small-slip regime) was first considered by Marble (1962, 1970). It was shown that to the main order of the small parameter L_{St}°/X° the dust velocity resembles closely that of the gas. The slip velocity is small and corresponds to the local gas acceleration. As the particles are 'frozen' into the gas, the dust density is conserved within the flow tubes. Since the upstream density is uniform, we have $N = N_\infty \left[1 + O\left(L_{St}^\circ/X^\circ\right)\right]$ for the entire flow, except for a small region near the leading edge at distances of the order of L_{St}° where the slip velocity is finite. The velocity and density fields in this small region were evaluated numerically by Osiptsov (1980). The particle density remains non-uniform within the flow tubes through the finite-slip zone. As a result in the region under investigation a thin layer close to the wall arises with non-uniform density distribution. Its thickness, $\delta_N^\circ \sim \delta^\circ (L_{St}^\circ/X^\circ)^{1/4}$, is small compared with the local thickness of the boundary layer, $\delta^\circ = (\nu^\circ X^\circ/U_\infty^\circ)^{1/2}$. Hence, it can be neglected to the main order of L_{St}°/X°.

For the small-slip regime with uniform particle distribution the equations of motion

https://doi.org/10.1017/S0022112098001256 Published online by Cambridge University Press

of the two phases may be combined to eliminate the momentum-transfer terms. As a result the solution for the mean dusty-gas flow is the same as that for a clean gas but with the fluid density changed from ρ° to $\rho^\circ(1+f)$ (Marble 1962, 1970), where

$$f = \frac{4\pi}{3} a^{\circ 3} N_\infty \frac{\rho_p^\circ}{\rho^\circ}$$

is the dimensionless particle mass content. For the problem in question the velocity field can be expressed in terms of the classical Blasius solution.

To solve the stability problem for a clean-gas boundary layer the approach of quasi-parallel and quasi-homogeneous (in the x-coordinate) mean flow is widely used (Schlichting 1968; Lin 1955). It yields stability characteristics that agree well with those from the solution of the three-dimensional linearized Navier–Stokes equations and the experiments. The approach is based on the assumption that the characteristic wavelength of the TS wave is of the order of the local thickness of the boundary layer δ° and small compared with the characteristic distance from the leading edge of the plate. The Reynolds number based on δ° is assumed to be large but finite, so that the mean-flow normal velocity is taken to be much less than the streamwise velocity, and the mean flow is considered as plane and parallel.

The same approach can also be successfully used for the stability problem of dusty-gas flow. We assume that the characteristic wavelength of the TS wave, L_{TS}°, is of the order of the relaxation length of the particle velocity, L_{St}°, and small compared with the distance X°. As shown in § 8 this requirement is fulfilled when the particle radius a° is sufficiently small (up to 10^{-6} m at normal conditions and upstream velocity $U_\infty^\circ = 100$ m s^{-1}). Although the mean-flow dust velocity to the main order equals that of the gas, the regime of finite slip occurs for the disturbance flow because $L_{St}^\circ \sim L_{TS}^\circ$.

To non-dimensionalize the governing equations we take the free-stream velocity U_∞°, the gas density ρ° and the local thickness of the clean-gas boundary layer δ° as the basic dimension variables. All other variables are scaled by some combination of these values.

Within the framework of the quasi-parallel and quasi-homogeneous approach we have for the dimensionless mean flow

$$U_x = V_x = U, \quad U_y = V_y = 0,$$

where

$$U(y) = U_0(\beta y) \tag{2.1}$$

is the mean-flow profile. Here $\beta = (1+f)^{1/2}$; subscript 0 characterizes hereinafter the parameters of a clean-gas flow, $U_0(y)$ is the Blasius velocity profile (Schlichting 1968).

The dimensionless Navier–Stokes equations for the two-dimensional perturbations of the gas flow then can be written as (Saffman 1962)

$$\frac{\partial u_x}{\partial x} + \frac{\partial u_y}{\partial y} = 0, \tag{2.2a}$$

$$\frac{\partial u_x}{\partial t} + U\frac{\partial u_x}{\partial x} + \frac{\mathrm{d}U}{\mathrm{d}y}u_y + \frac{\partial p}{\partial x} + fR\gamma\,(u_x - v_x) = \frac{1}{R}\left(\frac{\partial^2 u_x}{\partial x^2} + \frac{\partial^2 u_x}{\partial y^2}\right), \tag{2.2b}$$

$$\frac{\partial u_y}{\partial t} + U\frac{\partial u_y}{\partial x} + \frac{\partial p}{\partial y} + fR\gamma\,(u_y - v_y) = \frac{1}{R}\left(\frac{\partial^2 u_y}{\partial x^2} + \frac{\partial^2 u_y}{\partial y^2}\right), \tag{2.2c}$$

$$u_x(0) = u_y(0) = u_x(\infty) = u_y(\infty) = 0, \tag{2.2d}$$

https://doi.org/10.1017/S0022112098001256 Published online by Cambridge University Press

and the equations for the particle phase as

$$\frac{\partial f'}{\partial t} + U\frac{\partial f'}{\partial x} + f\left(\frac{\partial v_x}{\partial x} + \frac{\partial v_y}{\partial y}\right) = 0, \tag{2.3a}$$

$$\frac{\partial v_x}{\partial t} + U\frac{\partial v_x}{\partial x} + \frac{\mathrm{d}U}{\mathrm{d}y}v_y - R\gamma\,(u_x - v_x) = 0, \tag{2.3b}$$

$$\frac{\partial v_y}{\partial t} + U\frac{\partial v_y}{\partial x} - R\gamma\,(u_y - v_y) = 0, \tag{2.3c}$$

where

$$R = \frac{U_\infty^\circ \delta^\circ}{\nu^\circ}, \quad \gamma = \frac{9}{2}\left(\frac{U_\infty^\circ a^\circ}{\nu^\circ}\right)^{-2}\frac{\rho^\circ}{\rho_p^\circ}.$$

Here the space variables x, y are scaled by δ°, the velocities u_x, v_x, u_y, v_y by U_∞°, the pressure p by $\rho^\circ U_\infty^{\circ 2}$ and the time t by $\delta^\circ/U_\infty^\circ$. The last term on the left-hand side of each momentum equation is due to the Stokes momentum transfer between phases. Reynolds number R is based on the local boundary-layer thickness for a clean gas, and hence it is the same in the same sections of particle-free and dusty-gas flows. The dimensionless parameter γ is introduced instead of S given by (1.2). It characterizes the particle-phase features (particle size and density) and remains constant over the entire flow, while S varies with δ° which is taken as the length scale L_{TS}° of the flow.

It should also be noted that even though the disturbance of the particle density, $f' = \frac{4}{3}\pi a^{\circ 3} n\rho_p^\circ/\rho^\circ$, is assumed to be of the order of unity, it could be ignored for the problem considered. The reason is that the dimensionless mean-flow slip velocity is small for the small-slip regime, $|U_x - V_x|/U_x \ll 1$, while that for the disturbance flow is finite, $(u_x - v_x)/u_x = O(1)$. As a result, the terms containing f' in the linearized Navier–Stokes equations can be neglected in comparison with others (for example, we neglect $f'(U - V)$ in comparison with $f(u_x - v_x)$ in equation (2.2b)). Then the continuity equation for the dust (2.3a) is decomposed from other governing equations as for parallel flows (Saffman 1962; Michael 1964).

The flow disturbances $q = \left(u_x, u_y, p, v_x, v_y, f'\right)$ are sought in the form of a travelling wave, so that

$$q = q^* \exp(\mathrm{i}\alpha x - \mathrm{i}\omega t) + \text{c.c.}$$

Here the dimensionless wavenumber α and frequency ω of the wave are

$$\alpha = \alpha^\circ\delta^\circ, \quad \omega = \omega^\circ\delta^\circ/U_\infty^\circ,$$

where α is taken to be the real variable while ω is the complex one. Then (2.2) and (2.3) can be rewritten as

$$\mathrm{i}\alpha u_x^* + \frac{\mathrm{d}u_y^*}{\mathrm{d}y} = 0, \tag{2.4a}$$

$$\mathrm{i}(\alpha U - \omega)u_x^* + \frac{\mathrm{d}U}{\mathrm{d}y}u_y^* + \mathrm{i}\alpha p^* + fR\gamma\left(u_x^* - v_x^*\right) = \frac{1}{R}\left(\frac{\mathrm{d}^2 u_x^*}{\mathrm{d}y^2} - \alpha^2 u_x^*\right), \tag{2.4b}$$

$$\mathrm{i}(\alpha U - \omega)u_y^* + \frac{\mathrm{d}p^*}{\mathrm{d}y} + fR\gamma\left(u_y^* - v_y^*\right) = \frac{1}{R}\left(\frac{\mathrm{d}^2 u_y^*}{\mathrm{d}y^2} - \alpha^2 u_y^*\right), \tag{2.4c}$$

$$u_x^*(0) = u_y^*(0) = u_x^*(\infty) = u_y^*(\infty) = 0, \tag{2.4d}$$

https://doi.org/10.1017/S0022112098001256 Published online by Cambridge University Press

and

$$\mathrm{i}(\alpha U-\omega)v_x^*+\frac{\mathrm{d}U}{\mathrm{d}y}v_y^*-R\gamma\left(u_x^*-v_x^*\right)=0, \tag{2.5a}$$

$$\mathrm{i}(\alpha U-\omega)v_y^*-R\gamma\left(u_y^*-v_y^*\right)=0. \tag{2.5b}$$

The particle perturbed velocity can be readily expressed from (2.5) in terms of u_x^*, u_y^* as

$$v_x^*=\Lambda u_x^*-\frac{\Lambda^2}{R\gamma}\frac{\mathrm{d}U}{\mathrm{d}y}u_y^*,\quad v_y^*=\Lambda u_y^*, \tag{2.6}$$

where

$$\Lambda(y)=\left[1+\frac{\mathrm{i}\alpha}{R\gamma}(U-c)\right]^{-1}. \tag{2.7}$$

Here $c=\omega/\alpha$ is the complex phase velocity of the wave. From (2.4*a*) u_x^* can be expressed in terms of u_y^*. Then (2.4*b*), (2.4*c*) can be reduced to a modified Orr–Sommerfeld equation (Saffman 1962) given by

$$\mathrm{L}_{O-S}\left(\omega,\widetilde{U}\right)\varphi=0, \tag{2.8}$$

where

$$\mathrm{L}_{O-S}(\omega,U)=(U-c)\left(\frac{\mathrm{d}^2}{\mathrm{d}y^2}-\alpha^2\right)-\frac{\mathrm{d}^2U}{\mathrm{d}y^2}-\frac{1}{\mathrm{i}\alpha R}\left(\frac{\mathrm{d}^2}{\mathrm{d}y^2}-\alpha^2\right)^2,$$

and

$$\widetilde{U}=U+f\Lambda(U-c) \tag{2.9}$$

is the modified velocity profile. The boundary conditions for (2.8) are

$$\varphi(0)=0,\quad \frac{\mathrm{d}\varphi}{\mathrm{d}y}(0)=0,\quad \varphi(\infty)=0. \tag{2.10a–c}$$

The eigenfunction is normalized by

$$\frac{\mathrm{d}^2\varphi}{\mathrm{d}y^2}(0)=1. \tag{2.11}$$

The perturbations of the gas velocity are expressed in terms of φ as

$$u_x^*=\frac{\mathrm{d}\varphi}{\mathrm{d}y},\quad u_y^*=-\mathrm{i}\alpha\varphi.$$

Equation (2.8) differs from the ordinary Orr–Sommerfeld equation for a clean gas in that the fluid velocity $U(y)$ is replaced by the modified velocity profile $\widetilde{U}(y)$ which is a complex function of y. It should also be noted that the mean-flow velocity distributions $U(y)$ for dusty and clean gases were taken in previous investigations (Saffman 1962; Michael 1964; Yang *et al.* 1990) to be the same. This is valid, for example, for Poiseuille flow, since $U(y)$ does not depend on the density of the fluid. In our case, as seen from (2.1), the mean-flow velocity for the dusty gas differs from that for a clean gas.

Up to now we have considered only two-dimensional perturbations propagating in the streamwise direction. The three-dimensional case can be reduced to this one since the well-known Squire's theorem remains true for the dusty-gas stability problem (Saffman 1962). In the coordinate system with the $\hat{x}$-axis aligned in the direction of the wave propagation the linear stability problem is again governed by the modified

https://doi.org/10.1017/S0022112098001256 Published online by Cambridge University Press

Orr–Sommerfeld equation (2.8) with the boundary-layer velocity profile U being replaced by its component in the direction of the wave propagation.

Moreover, it can be shown that the complex frequency for the three-dimensional case can be expressed in terms of that for the two-dimensional flow calculated for other magnitudes of R, γ. In this case the component of the mean velocity in the $\widehat{x}$-direction is $\widehat{U}(y) = U(y)\cos\chi$ where χ is the angle between the streamwise direction and the direction of the wave propagation. Then introducing new variables

$$\widehat{\omega} = \omega/\cos\chi, \quad \widehat{R} = R\cos\chi, \quad \widehat{\gamma} = \gamma/\cos^2\chi,$$

one can transform the modified Orr–Sommerfeld equation with the mean velocity distribution $\widehat{U}$ to that with U. Finally, one can write

$$\omega_{3D} = \cos\chi\ \omega_{2D}\left(\alpha, R\cos\chi, f, \frac{\gamma}{\cos^2\chi}\right).$$

Therefore the stability characteristics of the three-dimensional perturbations ω_{3D} can be expressed in terms of those for the two-dimensional dusty-gas flow ω_{2D} with the same values of the wavenumber and the particle mass content but for smaller Reynolds number and greater γ. For this reason we consider below only the two-dimensional stability problem.

Our attention is focused first on the modification of the Tollmien–Schlichting (TS) wave due to the dust. The TS wave has attracted the most notice of the investigators of the stability problem for the clean gas as well. The reason is that it is a single unstable wave occurring in a boundary layer on a flat plate, while all other modes, including the continuous spectrum, are stable.

3. Limiting cases of fine ($\gamma \to \infty$) and coarse ($\gamma \to 0$) dust

The dependence $\omega(\alpha, R, f, \gamma)$ can be readily evaluated as $\gamma \to \infty$ or $\gamma \to 0$ if that for a clean-gas flow $\omega_0(\alpha, R)$ is known. For plane parallel flows these limiting cases were considered by Saffman (1962). It was shown that the addition of fine dust destabilizes the flow while coarse dust has a stabilizing effect. This conclusion remains qualitatively valid for the problem under consideration, but the parameters of the TS wave vary in some other way. This is due to the dissimilarity of the mean-flow velocity distribution $U(y)$ and $U_0(y)$ mentioned above (see (2.1)).

For fine particles the small-slip regime occurs for both the mean and disturbance flows. As a result, not only the solution for the mean flow, but also the solution of the linear stability problem are the same as those for a clean gas but with the fluid density changed from ρ° to $\rho^\circ(1+f)$. This conclusion follows also from (2.8). It can be easily verified that introducing new variables defined as

$$\widehat{y} = \beta y, \quad \widehat{\alpha} = \alpha/\beta, \quad \widehat{\omega} = \omega/\beta, \quad \widehat{R} = R\beta,$$

reduces (2.8) to the ordinary Orr–Sommerfeld equation with the mean-flow profile $U_0(y)$. Thus one can write $\widehat{\omega} = \omega_0(\widehat{\alpha}, \widehat{R})$ or

$$\omega(\alpha, R, f, \gamma) = \beta\omega_0\left(\frac{\alpha}{\beta}, \beta R\right) \quad \text{as} \quad \gamma \to \infty. \tag{3.1}$$

For the second limiting case $\gamma \to 0$ the mean-flow velocities of the two phases are equal, while the perturbed velocity of the coarse particles, as follows from (2.6), tends to zero. This means that they are not sensitive to rapid acceleration of the gas. As a

https://doi.org/10.1017/S0022112098001256 Published online by Cambridge University Press

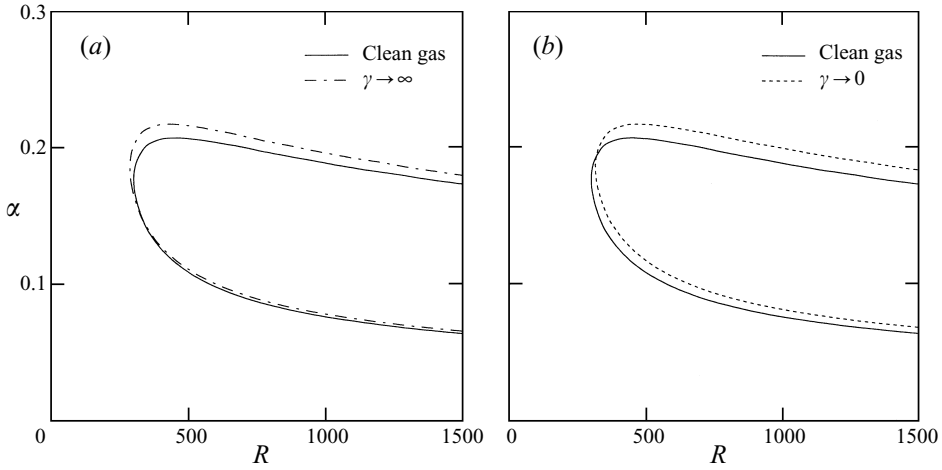


FIGURE 2. Neutral stability curves for (*a*) fine and (*b*) coarse particles at $f = 0.1$ in comparison with that for the clean gas (solid lines).

result particles experience the Stokes drag, and an equal but opposite volume force acts on the gas. Although in this case the unsteady slip velocity and the drag on a single particle are maximum, the dissipation of TS-wave energy due to the drag effect is negligible. The reason is that the volume density of the particles N decreases as $(a^\circ)^{-3}$ for given mass content f while the drag on a single particle grows only linearly with particle radius. Hence the increase in a° results in the terms in (2.2) and (2.9), corresponding to the unsteady momentum transfer, decreasing linearly with $(a^\circ)^{-2}$ or, equivalently, with γ. Therefore, the influence of the coarse dust on the stability characteristics is due only to the variation of the mean flow. Equation (2.8) again can be transformed to the ordinary Orr–Sommerfeld equation by introducing the new variables given by

$$\widehat{y} = \beta y, \quad \widehat{\alpha} = \alpha/\beta, \quad \widehat{\omega} = \omega/\beta, \quad \widehat{R} = R/\beta.$$

Finally we have

$$\omega(\alpha,\ R,\ f,\ \gamma) = \beta\omega_0\left(\frac{\alpha}{\beta},\ \frac{R}{\beta}\right) \quad \text{as} \quad \gamma \to 0. \tag{3.2}$$

The neutral stability curves in the (R,α)-plane for the fine and coarse particles calculated at $f = 0.1$ by conversion from those for a clean gas using (3.1) and (3.2) are presented in figure 2. It is seen that the addition of the fine particles reduces the critical Reynolds number while the coarse dust stabilizes the boundary-layer flow. For both limiting cases the characteristics of the instability wave are scarcely affected by particles. The dust effect is small at $\gamma \to \infty$ since the perturbed slip velocity and, hence, the Stokes drag are small. At $\gamma \to 0$ the Stokes drag on a single particle is sizeable but the number of particles N is small. As shown in the next section, dust may influence the perturbed flow significantly even at low particle mass content.

4. Exact numerical solution of the eigenvalue problem

The first approach used to solve numerically the eigenvalue problem for the modified Orr–Sommerfeld equation is direct integration of (2.8) using the orthonormalization

https://doi.org/10.1017/S0022112098001256 Published online by Cambridge University Press

method. It is applicable for arbitrary particle density. There are four linearly independent solutions of the fourth-order equation (2.8). Two of them denoted below as $\varphi_1(y)$, $\varphi_2(y)$ tend to zero on the upper edge of the boundary layer while the two others are unbounded. Then any solution meeting the boundary condition (2.10*c*) can be written as

$$\varphi = c_1\varphi_1 + c_2\varphi_2,$$

where c_1, c_2 are arbitrary constants. The numerical integration of (2.8) is started at sufficiently large y where the analytical expressions for φ_1, φ_2 can be obtained. Since $\widetilde{U}$ tends to a constant value at infinite y we have

$$\varphi_1 = \exp(-\alpha y), \quad \varphi_2 = \exp\left\{-\left(\mathrm{i}R\left[\alpha\widetilde{U}(\infty) - \omega\right] + \alpha^2\right)^{1/2} y\right\} \quad \text{as} \quad y \to \infty.$$

Two linearly independent solutions are integrated numerically down to the wall. When an independent solution becomes very large compared with the other significant reduction in the accuracy of the numerical solution occurs. This problem is eliminated by means of the orthonormalization method (Godunov 1961). Constants c_1, c_2 are determined to fulfil the boundary condition (2.10*a*) and the normalization condition (2.11). Thus we can write

$$c_1\varphi_1(0) + c_2\varphi_2(0) = 0, \quad c_1\frac{\mathrm{d}^2\varphi_1}{\mathrm{d}y^2}(0) + c_2\frac{\mathrm{d}^2\varphi_2}{\mathrm{d}y^2}(0) = 1.$$

The non-slip boundary condition on the wall (2.10*b*) in view of these equations can be rewritten as

$$D(\omega;\alpha,R,f,\gamma) = c_1\frac{\mathrm{d}\varphi_1}{\mathrm{d}y}(0) + c_2\frac{\mathrm{d}\varphi_2}{\mathrm{d}y}(0) = \frac{\varphi_1(0)\dfrac{\mathrm{d}\varphi_2}{\mathrm{d}y}(0) - \varphi_2(0)\dfrac{\mathrm{d}\varphi_1}{\mathrm{d}y}(0)}{\varphi_1(0)\dfrac{\mathrm{d}^2\varphi_2}{\mathrm{d}y^2}(0) - \varphi_2(0)\dfrac{\mathrm{d}^2\varphi_1}{\mathrm{d}y^2}(0)} = 0. \quad (4.1)$$

Equation (4.1) can be treated as an implicit dispersion relation. To evaluate the complex frequency ω explicitly, (4.1) is solved using the Newton method.

The distinction of the eigenvalue problem considered from that for a clean gas is that the modified velocity $\widetilde{U}(y)$ given by (2.9) depends on the unknown eigenvalue ω itself. Hence $\widetilde{U}(y)$ corresponding to the various modes are different for the same values of the mean-flow parameters. In order to illustrate this peculiarity consider TS mode $\omega = 0.0434 - \mathrm{i}0.0121$ and one of the stable modes $\omega = 0.0663 - \mathrm{i}0.0353$ calculated for $R = 1000$, $f = 1$, $\gamma = 10^{-4}$, $\alpha = 0.15$. The modified velocity profiles corresponding to these modes are shown in figure 3 in comparison with the Blasius velocity profile $U_0(y)$.

The numerical integration may also present some difficulty when $\mathrm{Im}(\omega) + R\gamma$ is small. The reason is that both real and imaginary parts of the denominator in equation (2.7) tend to zero in the critical layer where $U(y)$—$\mathrm{Re}(\omega/\alpha) \to 0$. Then the modified velocity $\widetilde{U}$ tends to infinity, and the regime outlined requires very small steps of integration since the eigenfunction varies rapidly in the critical layer. This difficulty is eliminated using the integration of (2.8) along the curved contour in the complex y-plane. Equation (2.8) has a singular point y_c if y is treated as a complex variable. Its position is governed by the equation

$$R\gamma + \mathrm{i}\alpha U(y_c) - \mathrm{i}\omega = 0. \quad (4.2)$$

To develop the numerical procedure we use the fact that the Blasius function and

https://doi.org/10.1017/S0022112098001256 Published online by Cambridge University Press

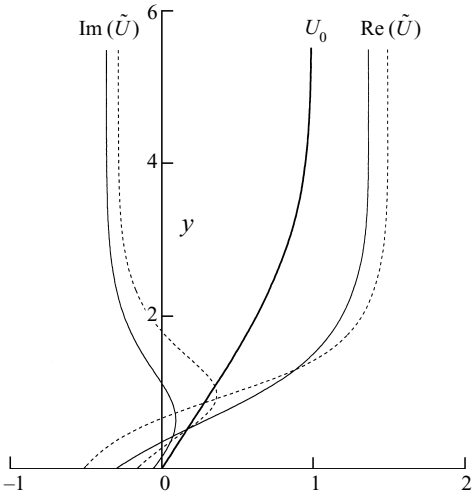


FIGURE 3. The modified velocity profiles at $R = 1000$, $f = 1$, $\gamma = 10^{-4}$, $\alpha = 0.15$ for the two modes $\omega = 0.0434 - i0.0121$ (solid lines) and $\omega = 0.0663 - i0.0353$ (dashed lines) in comparison with the Blasius velocity profile (heavy solid line).

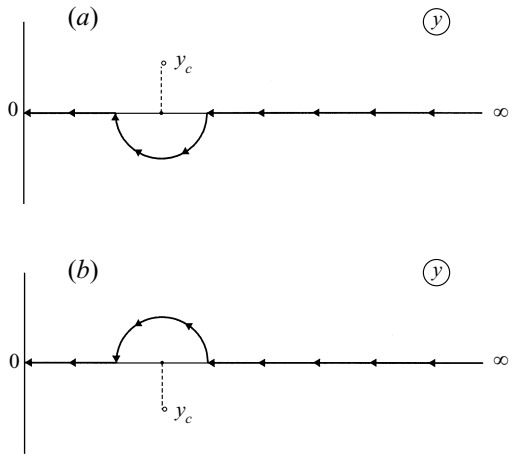


FIGURE 4. Integration contours of (2.8) for (*a*) Im $(\omega) > -R\gamma$ and (*b*) Im $(\omega) < -R\gamma$.

hence $U(y)$ are regular functions if y is complex. This makes it possible to integrate (2.8) along the curved contour in a complex y-plane. The integration is fulfilled along the contour shown in figure 4 which consists of segments of the real axis and a semi-circle passing round the point (Re (y_c), 0). The modified velocity remains finite everywhere on such a contour. The semi-circle is set on the upper semi-plane when Im $(\omega) < -R\gamma$ and on the lower semi-plane for the opposite inequality.

The complex frequency ω of the TS wave and eigenfunction were evaluated as functions of wavenumber α, Reynolds number R, parameter γ and dimensionless particle density f. The function Im (ω) calculated at $f = 0.1$, $\gamma = 10^{-4}$ is shown in the (R, α)-plane in figure 5(*a*) where its isolines are plotted. For comparison those for a clean gas are presented in figure 5(*b*). In contrast to the above limiting cases the dust's influence on the instability wave is significant. Not only is the critical Reynolds number essentially greater in this case, but also the growth rate of the TS wave is

https://doi.org/10.1017/S0022112098001256 Published online by Cambridge University Press

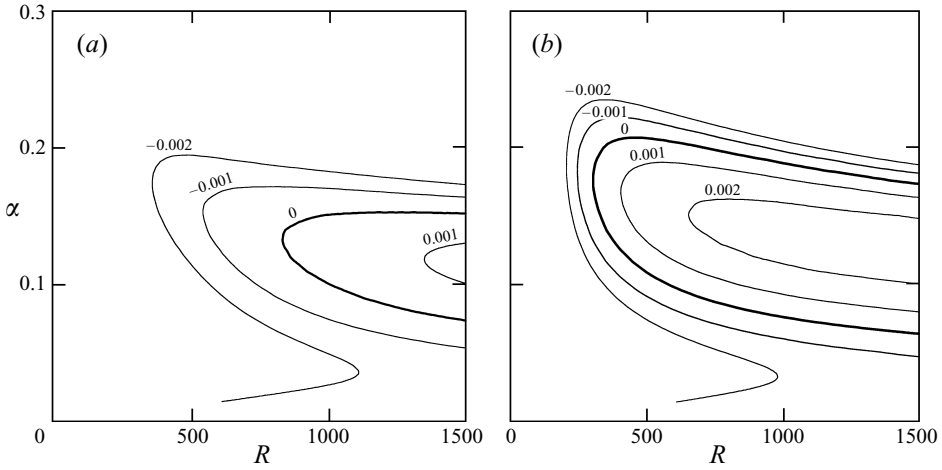


FIGURE 5. Isolines of $\mathrm{Im}\,(\omega)$ for (a) the dusty gas at $f = 0.1$, $\gamma = 10^{-4}$ and (b) clean gas. Heavy lines are the neutral stability curves ($\mathrm{Im}\,(\omega) = 0$).

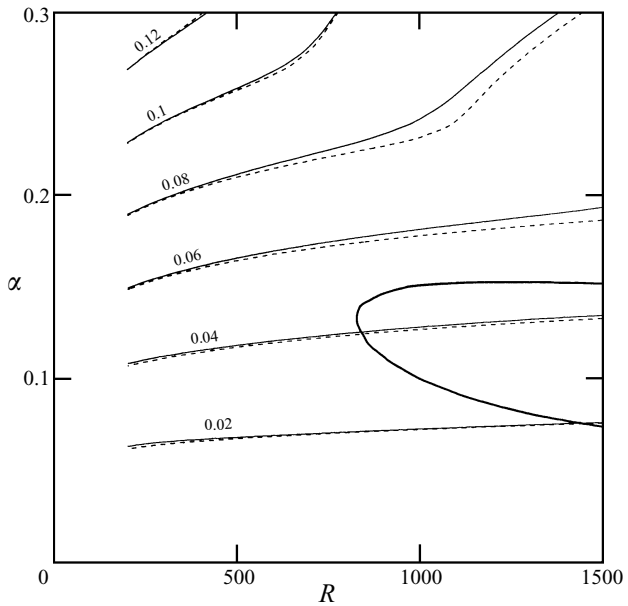


FIGURE 6. Isolines of $\mathrm{Re}\,(\omega)$ for the dusty gas at $f = 0.1$, $\gamma = 10^{-4}$ (solid lines) and clean gas (dashed lines).

reduced over the entire (R, α)-plane. So at $R = 1000$, $\alpha = 0.15$ the growth rate reduces from the value 0.002 28 estimated for a clean gas to 0.000 02 for the dusty gas. The isolines of the frequency $\mathrm{Re}\,(\omega)$ for clean (dashed lines) and dusty (solid lines) gases are shown in figure 6. The frequency of the TS wave varies on the addition of particles by considerably less than the growth rate.

Perturbed streamwise velocities of the gas and particles calculated at $R = 1000$, $f = 0.1$, $\gamma = 10^{-4}$, $\alpha = 0.15$ are shown in figure 7(a, b). The normal velocities are presented for the same parameters in figure 8(a, b). The value of the complex frequency in this case is $\omega = 0.0482 + \mathrm{i}\,0.227 \times 10^{-4}$, and the position of the singular point in the

https://doi.org/10.1017/S0022112098001256 Published online by Cambridge University Press

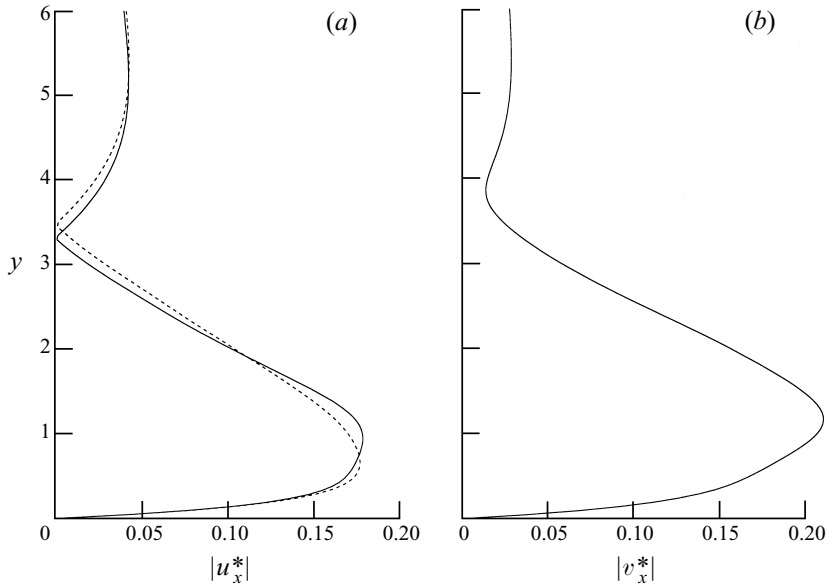


FIGURE 7. Magnitudes of the perturbed streamwise velocity vs. y at $R = 1000$, $f = 0.1$, $\gamma = 10^{-4}$, $\alpha = 0.15$ (a) of the dusty gas (solid line) in comparison with that for a clean gas (dashed line) and (b) of the particles.

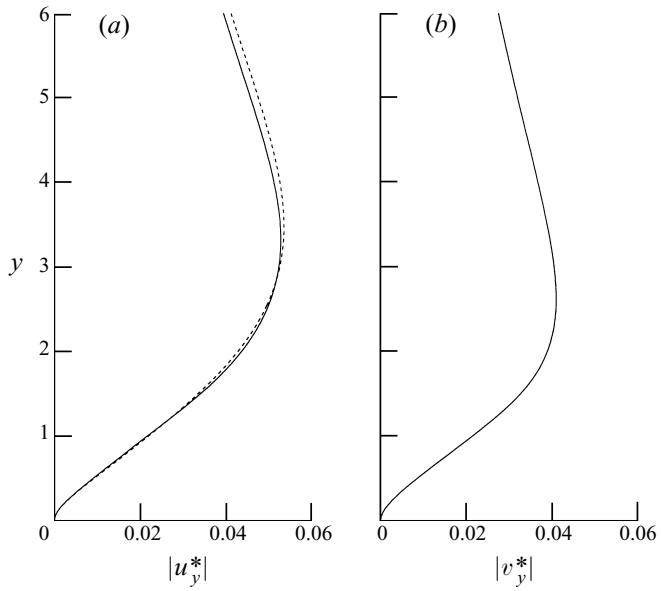


FIGURE 8. Magnitudes of the perturbed normal velocity vs. y (a) of the dusty gas and (b) of the particles. Parameters are the same as in figure 7.

complex y-plane is $y_c = 0.888 + \mathrm{i}\,1.783$. The variation of the gas velocity due to the dust with respect to the clean-gas case is small over the entire boundary layer.

The damping effect would be expected to be the maximum for some optimum γ. In this case the particle size is sufficiently small to make the particle concentration N large for given f and sufficiently large to maintain sizeable unsteady slip velocity and

https://doi.org/10.1017/S0022112098001256 Published online by Cambridge University Press

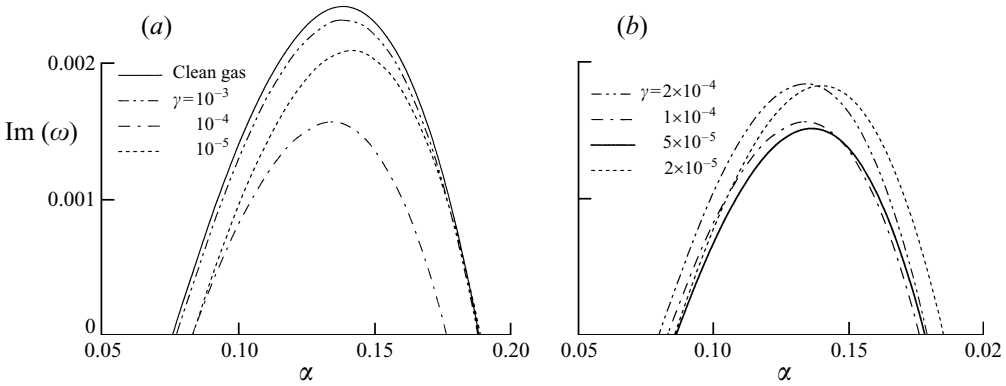


FIGURE 9. Growth rates vs. α at $R = 1000$, $f = 0.04$ and various γ.

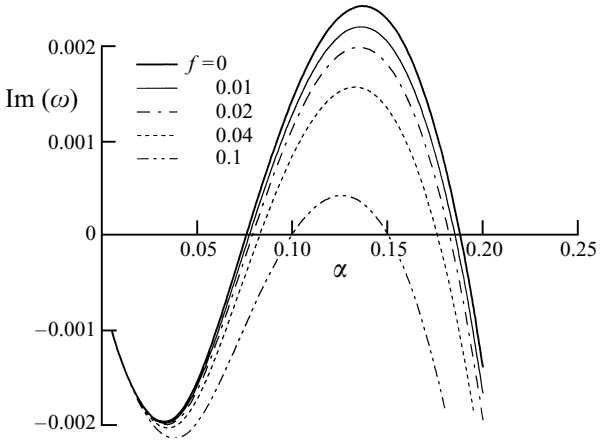


FIGURE 10. Growth rates vs. α at $R = 1000$, $\gamma = 10^{-4}$ and various f.

Stokes drag. The latter condition is fulfilled when the relaxation length of the particle velocity is of the order of the wavelength of the TS wave, or equivalently $\gamma \sim \alpha/R$. The dependence of $\mathrm{Im}\,(\omega)$ on α computed for $\gamma = 10^{-5}$, 10^{-4}, 10^{-3} and $R = 1000$, $f = 0.04$ is shown in figure 9(*a*). It is seen that the dust damps the TS wave for a wide range of γ. The maximum reduction in growth rate takes place for given R at $\gamma = 5 \times 10^{-5}$ (see figure 9*b*).

The dependence of the growth rate on particle mass content is illustrated in figures 10 and 11. In figure 10 $\mathrm{Im}\,(\omega)$ calculated as a function of α at $R = 1000$, $\gamma = 10^{-4}$ and $f = 0.01,\ 0.02,\ 0.04,\ 0.1$ are presented. Dust results in a significant reduction of growth rate even at small particle content. The f-dependence of $\mathrm{Im}\,(\omega)$ at $\alpha = 0.15$, $R = 1000$, $\gamma = 10^{-4}$ for the two discrete modes mentioned above is shown in figure 11. The dependence is nearly linear. This suggests the use of the second approach when the dust content is small, namely the perturbation method. Numerical procedure in this method is more simple but can be used only at small f.

5. Perturbation theory

At small particle content ($f \ll 1$) the eigenfunction and the eigenvalue of the modified Orr–Sommerfeld equation can be presented as a perturbation of those of

https://doi.org/10.1017/S0022112098001256 Published online by Cambridge University Press

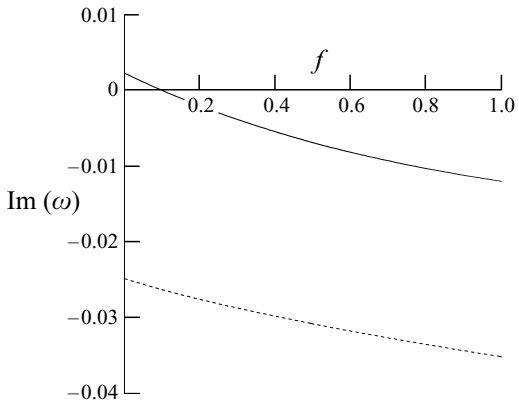


FIGURE 11. Dependence of $\mathrm{Im}\,(\omega)$ on f at $R = 1000$, $\gamma = 10^{-4}$, $\alpha = 0.15$ for the TS wave (solid line) and for the mode that is stable for a clean gas (dashed line).

the Orr–Sommerfeld equation for a clean gas. A solution of (2.8) is sought in the form

$$\varphi = \varphi_0 + f\varphi_1 + O\left(f^2\right), \quad \omega = \omega_0 + f\omega_1 + O\left(f^2\right), \tag{5.1}$$

where φ_0, ω_0 is the solution of the ordinary Orr–Sommerfeld equation for a clean gas given by

$$\mathrm{L}_{O-S}\left(\omega_0, U_0\right)\varphi_0 = 0, \quad \varphi_0\left(0\right) = \frac{\mathrm{d}\varphi_0}{\mathrm{d}y}\left(0\right) = \varphi_0\left(\infty\right) = 0.$$

The modified velocity profile can also be presented in terms of series of f so that

$$\widetilde{U}(y) = U_0(y) + fU_1(y) + O(f^2), \tag{5.2}$$

where

$$U_1 = \frac{y}{2}\frac{\mathrm{d}U_0}{\mathrm{d}y} + \Lambda_0\left(U_0 - c_0\right). \tag{5.3}$$

The first term in (5.3) is due to the variation of the mean-velocity distribution with respect to a particle-free flow, and the second one is due to the momentum transfer between phases. Thus (5.2) accounts for the dust's influence both on the mean and the perturbation flows. The perturbation of the complex frequency is determined from the following equation:

$$\omega_1 = -\frac{\left(\varphi_0^+, \mathrm{L}_{U_1}\varphi_0\right)}{\left(\varphi_0^+, \mathrm{L}_{\omega}\varphi_0\right)}, \tag{5.4}$$

where

$$\left(\psi, \varphi\right) = \int_0^\infty \overline{\psi}\varphi\,\mathrm{d}y,$$

$$\mathrm{L}_{U_1} = U_1\left(\frac{\mathrm{d}^2}{\mathrm{d}y^2} - \alpha^2\right) - \frac{\mathrm{d}^2U_1}{\mathrm{d}y^2}, \quad L_\omega = -\frac{1}{\alpha}\left(\frac{\mathrm{d}^2}{\mathrm{d}y^2} - \alpha^2\right).$$

Here the overbar denotes the complex conjugated value. The adjoint function φ_0^+ is governed by the boundary-value problem:

$$\mathrm{L}_{O-S}^+\left(\omega_0, U_0\right)\varphi_0^+ = 0, \quad \varphi_0^+\left(0\right) = \frac{\mathrm{d}\varphi_0^+}{\mathrm{d}y}\left(0\right) = \varphi_0^+\left(\infty\right) = 0, \tag{5.5a,b}$$

https://doi.org/10.1017/S0022112098001256 Published online by Cambridge University Press

where

$$\mathrm{L}^{+}_{O-S}(\omega, U) = (U - \bar{c})\left(\frac{\mathrm{d}^2}{\mathrm{d}y^2} - \alpha^2\right) + 2\frac{\mathrm{d}U}{\mathrm{d}y}\frac{\mathrm{d}}{\mathrm{d}y} + \frac{1}{\mathrm{i}\alpha R}\left(\frac{\mathrm{d}^2}{\mathrm{d}y^2} - \alpha^2\right)^2$$

is the adjoint operator.

The solution φ_0^+ of (5.5) is sought using the othonormalization method. The variation of the modified velocity, U_1, as well as of $\widetilde{U}$, has a pole in the complex y-plane. As a result the integrand of the integral in the numerator of (5.4) also has a pole y_{c0} defined by

$$R\gamma + \mathrm{i}\alpha U(y_{c0}) - \mathrm{i}\omega_0 = 0. \tag{5.6}$$

When $\mathrm{Im}(\omega_0) + R\gamma \to 0$, and the pole is in the vicinity of the real y-axis, the integration in both the numerator and denominator of (5.4) is performed along the curved contours shown in figure 4. The calculations of the complex frequency of the TS wave is simpler in the framework of the perturbation method than those using direct integration. Once computed the functions φ_0^+, φ_0 are used to evaluate ω_1 for different values of γ.

For the limiting case $\gamma \to 0$ the second term in (5.3) tends to zero. Hence this case represents the variation of the growth rate due to a change in the mean velocity only. Also, ω_1 can be readily evaluated from (3.2) obtained for finite dust content. The differentiation of (3.2) with respect to f gives

$$\omega_1 = \frac{1}{2}\left(\omega_0 - \alpha\frac{\partial\omega_0}{\partial\alpha} - R\frac{\partial\omega_0}{\partial R}\right) \quad \text{as} \quad \gamma \to 0.$$

For the opposite limiting case of fine particles one can obtain from (3.1)

$$\omega_1 = \frac{1}{2}\left(\omega_0 - \alpha\frac{\partial\omega_0}{\partial\alpha} + R\frac{\partial\omega_0}{\partial R}\right) \quad \text{as} \quad \gamma \to \infty.$$

The isolines of $\mathrm{Im}(\omega_1)$ in the (R, α)-plane for the coarse ($\gamma \to 0$) and fine ($\gamma \to \infty$) dust are shown in figure 12 (a, b) respectively. The solid heavy lines are the neutral stability curves for a clean gas, and the dashed curves correspond to $\mathrm{Im}(\omega)_1 = 0$. It can be seen that for both cases there are the regions in the lower parts of the (R, α)-plane where $\mathrm{Im}(\omega_1) < 0$. Hence both the fine and the coarse dusts stabilize the TS wave at small α. This region where the growth rate is reduced because of the dust, is greater for $\gamma \to 0$ and includes the neighbourhood of the critical point (R_c, α_c). For the fine dust we have $\mathrm{Im}(\omega_1) > 0$ in the vicinity of the critical point.

In figure 12(c) $\mathrm{Im}(\omega_1)$ calculated at $\gamma = 5 \times 10^{-5}$ is shown. The reduction in growth rate per unit of dust content for this optimum regime is approximately ten times greater than the characteristic value of the growth rate itself. Note that the minimum of $\mathrm{Im}(\omega_1)$ is in the middle of the unstable region in the (R, α)-plane.

A comparison of results of both methods shows that the perturbation theory can be successfully used to calculate the characteristics of the TS wave. This conclusion is illustrated for unstable waves in figure 13 where $\mathrm{Re}(\omega)$ and $\mathrm{Im}(\omega)$ yielded by direct integration and the perturbation theory are shown as functions of the dust content at $R = 1000$, $\gamma = 10^{-4}$, $\alpha = 0.15$. The perturbation theory predicts well the growth rates up to $f = 0.1$ and the frequency of the TS wave up to $f = 1$.

https://doi.org/10.1017/S0022112098001256 Published online by Cambridge University Press

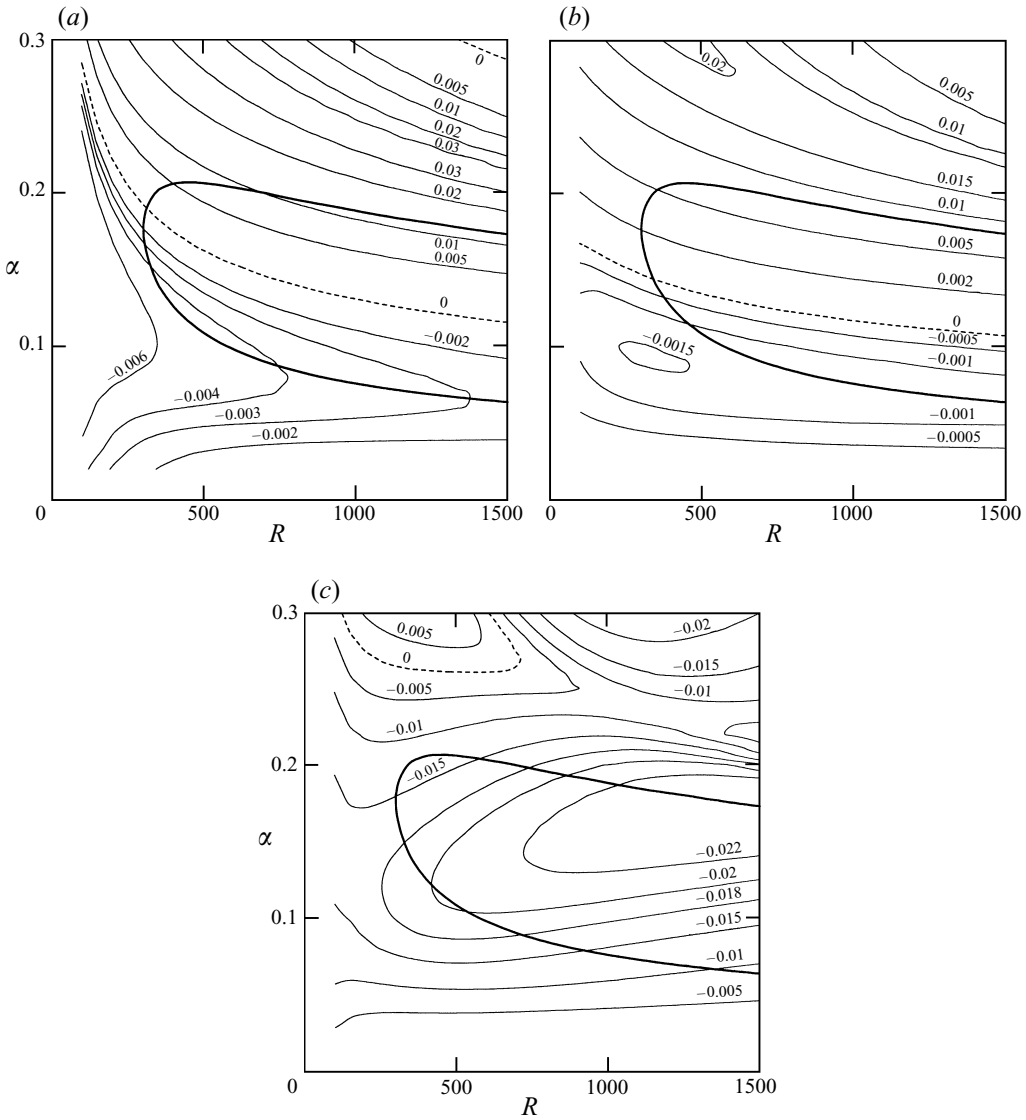


FIGURE 12. Isolines of $\mathrm{Im}\,(\omega_1)$ for (*a*) $\gamma \to 0$ (coarse dust), (*b*) $\gamma \to \infty$ (fine dust) and (*c*) $\gamma = 5 \times 10^{-5}$. Dashed curves are the lines where $\mathrm{Im}\,(\omega_1) = 0$, solid heavy lines are the neutral stability curves for a clean gas.

6. Discontinuity of the eigenvalue

The discontinuity of the eigenvalue is due to the fact that the modified velocity $\widetilde{U}$ has a pole y_c in the complex y-plane given by (4.2). By this is meant that y_c is a branch point for the solution of the modified Orr–Sommerfeld equation (2.8). The complex frequency ω is an analytical function of α, R, f, γ till y_c remains on the same semi-plane of the complex y-plane: on the upper semi-plane when $\mathrm{Im}\,(\omega) + R\gamma > 0$ or on the lower semi-plane for the opposite inequality. However at some α, R, f, γ the singular point crosses the real y-axis. Then the solution of the eigenvalue problem changes in a discontinuous way. We define $\omega^{(+)}$ and $\omega^{(-)}$ as the analytical solutions of (2.8) corresponding to the upper and lower positions of the singular point.

https://doi.org/10.1017/S0022112098001256 Published online by Cambridge University Press

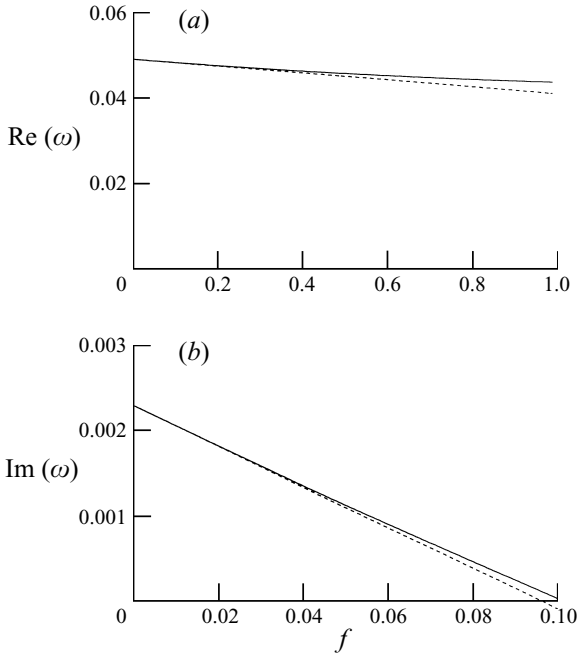


FIGURE 13. Comparison of the dependences of (*a*) $\mathrm{Re}\,(\omega)$ and (*b*) $\mathrm{Im}\,(\omega)$ on f calculated using direct integration (solid lines) and perturbation theory (dashed lines) at $R = 1000$, $\gamma = 10^{-4}$, $\alpha = 0.15$.

The physical cause of the phenomenon is a resonant acceleration of the particles in a critical layer. As follows from (2.6) and (2.7), Λ, v_x^*/u_x^* and v_y^*/u_y^* tend to infinity when the branch point approaches the real y-axis, or, equivalently, $\mathrm{Im}\,(\omega)$ tends to the resonant value $(-R\gamma)$. The effect arises only at $\mathrm{Im}\,(\omega) < 0$, that is for stable eigenmodes. It should be noted that the perturbed particle velocity scaled by the amplitude of perturbations ϵ can be as large as wished. However it assumed to be small compared with $\epsilon^{-1} \gg 1$, so that the perturbation remains small compared with the main-flow velocity.

The discontinuity appears also when the stability problem is solved approximately in the framework of the perturbation method. The variation of the complex frequency ω_1 becomes discontinuous when y_{c0} crosses the real y-axis.

6.1. *Perturbation method*

The integrand of the numerator of (5.4) $\overline{\varphi_0^+}\mathrm{L}_{U_1}\varphi_0$ has a pole y_{c0} given by (5.6). The pole locations calculated at $\gamma = 10^{-5}$, $R = 1000$ and several values of α are shown in a complex y-plane in figure 14. A pole lies on the real y-axis, that is, the solution of (5.6) is real when its real part equals zero, or equivalently

$$\mathrm{Im}\,(\omega_0(\alpha, R)) + R\gamma = 0. \tag{6.1}$$

This equation is satisfied on some line l in (R, α)-plane, as shown in figure 15 for $\gamma = 10^{-5}$ by the dashed-and-dotted line. This line separates the (R, α)-plane into the region in which the pole y_{c0} is on the upper semi-plane (to the right of l) and the region with the lower pole position (above and to the left of l).

The integrals in the numerator of (5.3) calculated for two nearby points on different sides of l differ by a finite value. As a result the distribution $\omega_1(\alpha, R)$ shown in figure 15 has discontinuity on l. The jump condition can be calculated using the integral

https://doi.org/10.1017/S0022112098001256 Published online by Cambridge University Press

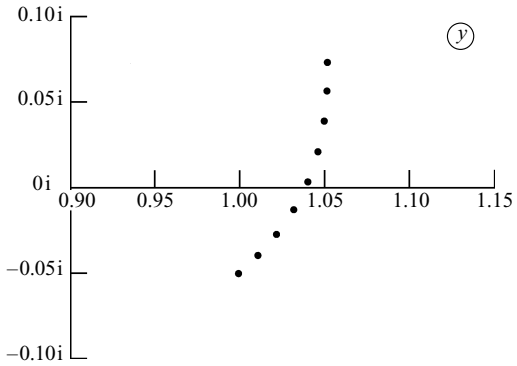


FIGURE 14. The pole positions of $\overline{\varphi_0^+}\mathrm{L}_{U_1}\varphi_0$ (the integrand of the numerator of (5.4)) at $\gamma = 10^{-5}$, $R = 1000$ and different α. The wavenumber increases from $\alpha = 0.22$ (the topmost symbol) to 0.26 with step $\Delta\alpha = 0.005$.

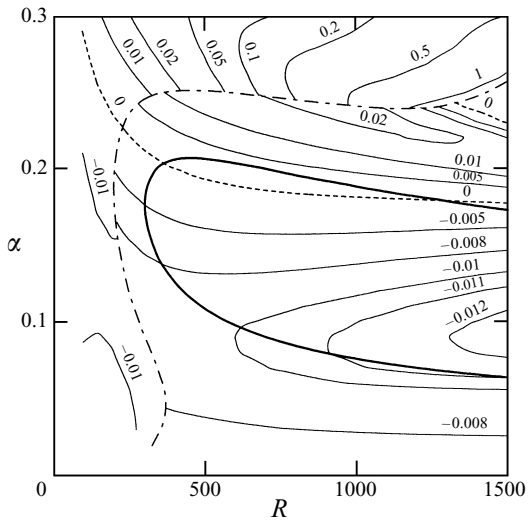


FIGURE 15. Isolines of $\mathrm{Im}\,(\omega_1)$ at $\gamma = 10^{-5}$. The lines break on curve l (dashed-and-dotted line). The dashed curves are the lines where $\mathrm{Im}\,(\omega_1) = 0$, solid heavy line is the neutral stability curve for a clean gas.

Cauchy's theorem. The difference of two integrals equals the residue in y_{c0} multiplied by $2\pi\mathrm{i}$. Finally we have

$$[\omega_1] = \omega_1^{(+)} - \omega_1^{(-)} = 2\pi\mathrm{i}\left(\frac{R\gamma}{\alpha}\right)^2 \frac{\Phi(y_{c0})}{(\varphi_0^+, L_\omega\varphi_0)} \quad \text{on} \quad l, \tag{6.2}$$

where

$$\Phi = \left(\alpha^2\varphi_0\overline{\varphi_0^+} + 2\frac{\mathrm{d}\varphi_0}{\mathrm{d}y}\frac{\mathrm{d}\overline{\varphi_0^+}}{\mathrm{d}y} + \varphi_0\frac{\mathrm{d}^2\overline{\varphi_0^+}}{\mathrm{d}y^2}\right)\left(\frac{\mathrm{d}U_0}{\mathrm{d}y}\right)^{-1}.$$

The perturbation theory can also be used to predict the growth rate for the case when the growth rate is less than the resonant value $(-R\gamma)$. It deviates from the linear dependence at lower values of f than for the unstable TS wave. The reason is that $\omega_1^{(+)}$ for given R, α is much greater than the characteristic values of $\omega_1^{(-)}$.

https://doi.org/10.1017/S0022112098001256 Published online by Cambridge University Press

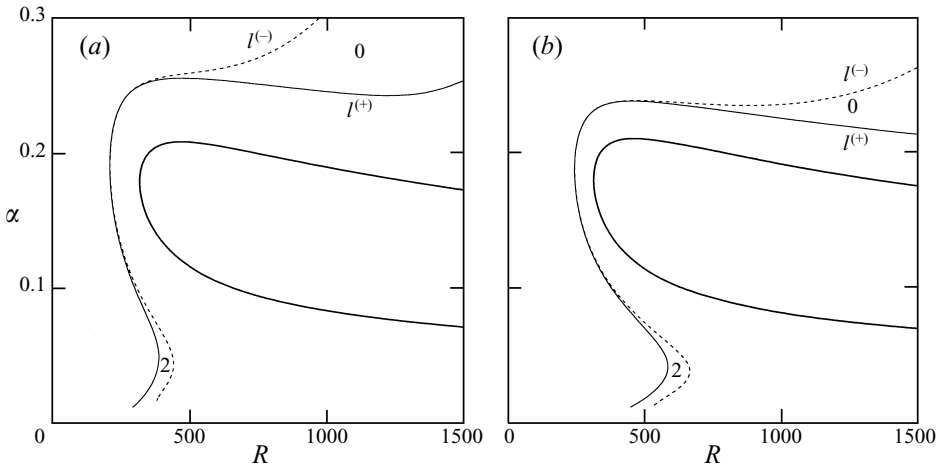


FIGURE 16. The regions in the (R, α)-plane with the upper (to the right of the curve $l^{(+)}$) and lower (above and to the left of the curve $l^{(-)}$) positions of the singular point at $f = 0.04$: (*a*) $\gamma = 10^{-5}$ and (*b*) $\gamma = 5 \times 10^{-6}$. The two discrete TS modes exist in the domain marked 2 where these regions overlap. In a gap between two regions marked 0 no TS mode may exist.

6.2. *Direct integration*

In the framework of the perturbation theory we obtain the discontinuity of the eigenvalue when α, R, γ satisfy equation (6.1). The points in the (R, α)-plane corresponding to the limiting upper and lower pole positions are on different sides of the same line l. Note that y_{c0} is determined from the solution of the eigenvalue problem for a clean gas. When the discontinuity is considered at finite f in the framework of the direct integration of the modified Orr–Sommerfeld equation, the sign of the expression $\mathrm{Im}\,(\omega) + R\gamma$ and hence the position of y_c is not known *a priori* but depends on the solution of the eigenvalue problem itself. As a result the solutions of equations

$$\mathrm{Im}\ (\omega(\alpha, R, f, \gamma)) + R\gamma = +0, \tag{6.3}$$

$$\mathrm{Im}\ (\omega(\alpha, R, f, \gamma)) + R\gamma = -0, \tag{6.4}$$

governing the limiting upper and lower positions of the singular point are not identical. Thus we have two lines in the (R, α)-plane where y_c is on the real y-axis. In figure 16 two curves $l^{(+)}$ and $l^{(-)}$ (solid and dashed lines respectively), on which (6.3) and (6.4) are satisfied, are shown for $f = 0.04$ and (*a*) $\gamma = 10^{-5}$ and (*b*) $\gamma = 5 \times 10^{-6}$. The region with the upper singular point is to the right of $l^{(+)}$ while that with the lower position is above and to the left of $l^{(-)}$. The two regions overlap in the domain marked 2. Two discrete TS modes $\omega^{(+)}$ and $\omega^{(-)}$ exist here. A gap occurs between the two regions marked 0 where no TS mode may exist. The discontinuity region is closer to the neutral stability curve at smaller values of γ (see figure 16*b*). The discontinuity of the eigenvalue is also illustrated on figure 17 where the dependence on $\mathrm{Im}\,(\omega)$ of α calculated at $\gamma = 5 \times 10^{-6}$, $f = 0.04$, (*a*) $R = 500$ and (*b*) $R = 1000$ is presented. It is seen on figure 17(*a*) that there are two intervals of α at $R = 500$ where two discrete TS modes exist. So at $\alpha = 0.072$ we have two modes of the TS wave: $\omega^{(-)} = 0.0218 - \mathrm{i}\,0.002\,60$ and $\omega^{(+)} = 0.0218 - \mathrm{i}\,0.002\,39$. The profiles of the perturbed streamwise velocities for these two modes are shown in figure 18. The derivative of one eigenfunction grows rapidly while that of the other reduces rapidly in a narrow region in the critical layer (near $y = 0.9$). This results in the eigenfunctions differing

https://doi.org/10.1017/S0022112098001256 Published online by Cambridge University Press

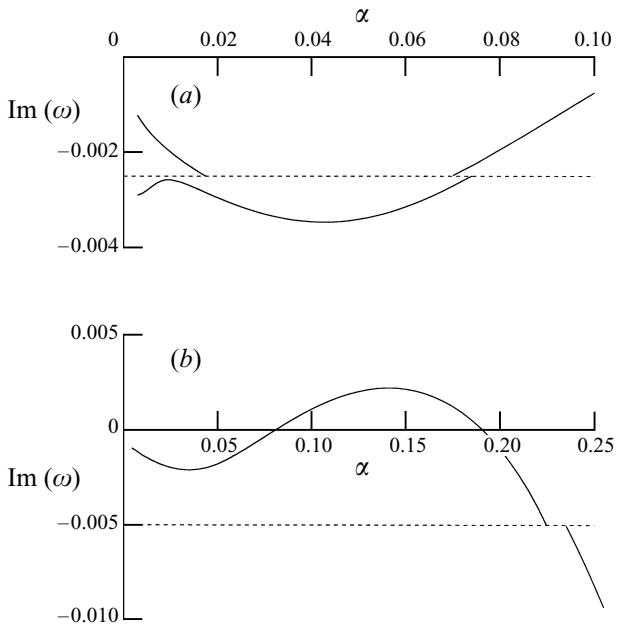


FIGURE 17. Im(ω) vs. α at $\gamma = 5 \times 10^{-6}$, $f = 0.04$: (*a*) $R = 500$ and (*b*) $R = 1000$. Curves break at resonant values $(-R\gamma)$ (dashed line). There are two intervals at $R = 500$ where two discrete TS modes exist. At $R = 1000$ there is an interval where the eigenvalue problem has no solution.

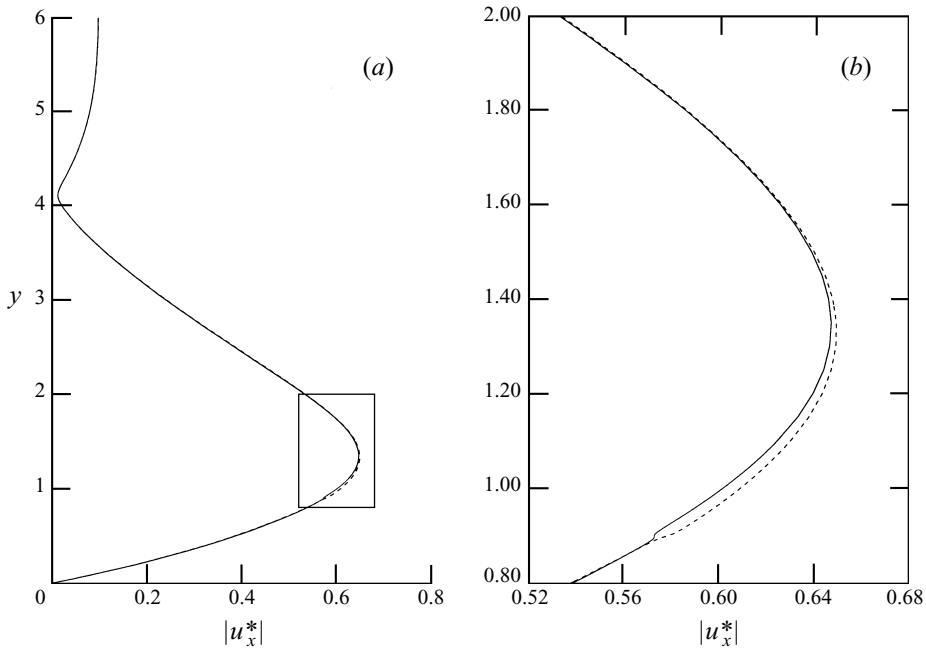


FIGURE 18. (*a*) Magnitudes of the perturbed streamwise velocities vs. y for the two modes of the TS wave $\omega^{(-)} = 0.0218 - \mathrm{i}\,0.002\,60$ (solid lines) and $\omega^{(+)} = 0.0218 - \mathrm{i}\,0.002\,39$ (dashed lines) at $R = 500$, $\alpha = 0.072$, $\gamma = 5 \times 10^{-6}$, $f = 0.04$. (*b*) An expanded view of the boxed region in (*a*).

https://doi.org/10.1017/S0022112098001256 Published online by Cambridge University Press

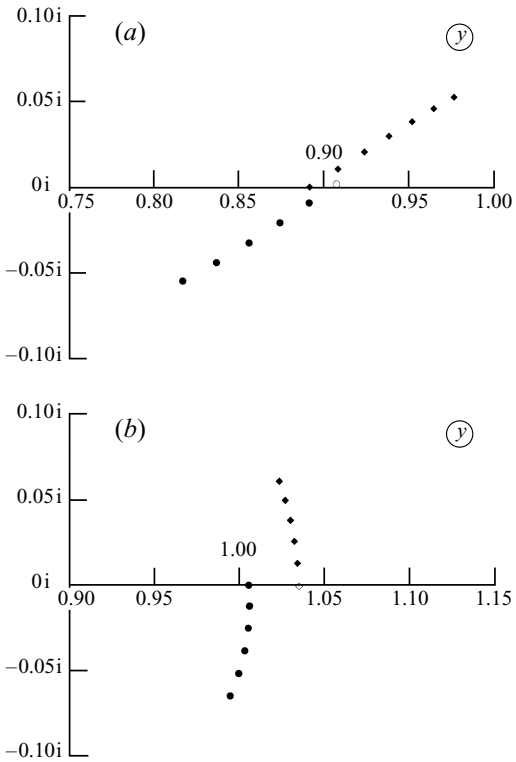


FIGURE 19. The singular point positions in the complex y-plane at $\gamma = 5\times10^{-6}$, $f = 0.04$: (a) $R = 500$ and (b) $R = 1000$. ◆, ◇ and ●, ○ are calculated using the integration along the contours shown in figures 4(a) and 4(b) respectively. Wavenumber increases for all sets of the singular points with step $\Delta\alpha = 0.005$: (a) ●, ○ $\alpha = 0.05$ (the bottom symbol) to 0.075; ◇ 0.07 (the bottom symbol) to 0.1; (b) ◆, ◇ 0.2 (the topmost symbol) to 0.225; ● 0.235 (the topmost symbol) to 0.26.

noticeably in the region above the critical layer. The reason why they are close near the wall is the normalization condition (2.11). In figure 17(b) there is an interval where the eigenvalue problem has no solution.

The singular point positions in the complex y-plane for the same γ, f, R and several α are shown in figure 19(a,b). The singular points marked by circles are obtained using the integration along the contour shown in figure 4(a) while those marked by diamonds are evaluated using the integration contour shown in figure 4(b). Since the pole position is not known *a priori* we also have no prior knowledge of what integration contour should be used. At some values of α, R one may obtain a solution with a singular point lying between the integration contour and the real y-axis (open symbols). Such a solution does not make it possible to transform the integration contour into the real y-axis with the eigenfunction remaining a regular function, and for this reason it must be rejected.

The regions in the (R,α)-plane where two modes arise or the eigenvalue problem has no solution can also be found approximately using the perturbation method. The solution for ω given by (5.1) is valid in the vicinity of l at $f \to 0$. One can calculate approximately the new position of the singular point from (4.2) by replacing ω by $\omega_0 + f\omega_1$. Then the lines $l^{(+)}$ and $l^{(-)}$ corresponding to the limiting upper and lower

https://doi.org/10.1017/S0022112098001256 Published online by Cambridge University Press

pole positions with an accuracy of $O\left(f^2\right)$ are governed by the equations

$$\mathrm{Im}\left[\omega_0 + f\omega_1^{(+)}\right] + R\gamma = 0, \quad \text{and} \quad \mathrm{Im}\left[\omega_0 + f\omega_1^{(-)}\right] + R\gamma = 0.$$

The overlap and the gap intervals $\Delta\alpha$ for given R (see figure 17) can be also calculated at small f from the following equation:

$$\Delta\alpha = f\ \mathrm{Im}\left[\omega_1\right]\left|\frac{\partial \mathrm{Im}\left(\omega_0\right)}{\partial\alpha}\right|^{-1} + O(f^2). \tag{6.5}$$

Here the jump condition for ω_1 is given by (6.2), and the derivative of $\mathrm{Im}\left(\omega_0\right)$ is evaluated on l. The overlapping arises when $\Delta\alpha$ is positive, while the gap corresponds to $\Delta\alpha < 0$.

7. Polydisperse dust

The above considerations can be extended to the boundary-layer flow containing particles of different sizes. The effect is considered below for both discrete and continuous distributions in the particle size. The relaxation lengths of all particles are assumed to be of the order of the characteristic wavelength and small compared with the distance from the leading edge, so that the quasi-homogeneous approach again can be used.

7.1. *Discrete distribution*

The dust is divided into several groups with various sizes a_j and uniform upstream volume densities N_j. Each size group is characterized by its own parameter

$$\gamma_j = \frac{9}{2}\left(\frac{U_\infty^\circ a_j^\circ}{\nu^\circ}\right)^{-2}\frac{\rho^\circ}{\rho_p^\circ}.$$

The mass fraction F_j of the particles of size a_j° is introduced by $F_j = N_j a_j^{\circ 3}/\sum_j N_j a_j^{\circ 3}$ so that $\sum_j F_j = 1$. Then equation (2.6) for the perturbed velocity for any particle size remains true but the function Λ given by (2.7) should be replaced by $\Lambda_j = [1 + \mathrm{i}\alpha(U-c)/R\gamma_j]^{-1}$. The corresponding sum should replace each term due to the dust influence in the equations governing the gas velocity and pressure perturbations, that is, any term $f\Gamma\left(y;\gamma\right)$ in (2.4), (2.9) depending on γ should be replaced by $f\sum_j F_j\Gamma\left(y;\gamma_j\right)$. The linear stability in this case is governed by the modified Orr–Sommerfeld equation with $\widetilde{U}$ given by

$$\widetilde{U} = U + f\left(U-c\right)\sum_j F_j\Lambda\left(y;\gamma_j\right).$$

This modified velocity profile has several poles, $y_c\left(\gamma_j\right)$, in the complex y-plane, with their number being equal to the number of particle sizes. For the unstable TS wave all of them are on the upper semi-plane. Therefore we can use a numerical scheme similar to that described in § 4. The calculations of the eigenvalues show that the damping effect of the polydisperse dust is similar to the monodisperse case, and the most efficient suppression is provided by the particles with relaxation length close to the TS wavelength. The growth rate for dust containing particles of three sizes are presented in figure 20. The stabilizing effect is only slightly less than for the near-optimum monosized dust with $\gamma = 10^{-4}$.

The discontinuity effect is more complicated for the polydisperse dust than for the

https://doi.org/10.1017/S0022112098001256 Published online by Cambridge University Press

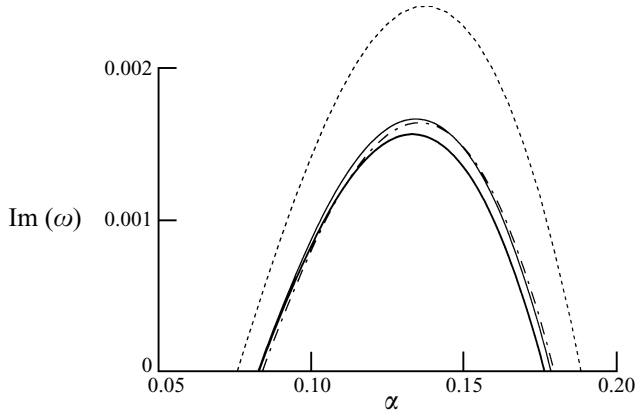


FIGURE 20. The growth rates for polydisperse dust at $R = 1000$, $f = 0.04$ in comparison with monosized dust with $\gamma = 10^{-4}$ (heavy solid line) and a clean-gas (dashed line) case. Dashed-dotted line corresponds to dust containing particles of three sizes with $\gamma_1 = 0.5 \times 10^{-4}$, $\gamma_2 = 1 \times 10^{-4}$, $\gamma_3 = 1.5 \times 10^{-4}$; $F_1 = F_3 = 0.25$, $F_2 = 0.5$; and the thin solid line to the continuous distribution given by (7.2) at $\gamma_0 = 10^{-4}$, $\Delta\gamma = 0.5 \times 10^{-4}$. The maxima of growth rates for both distributions are slightly higher than that for the near-optimum monosized case.

monosized case, since for the stable TS wave the poles may be on both the upper and lower semi-planes. The path of integration along the real y-axis is clamped between them in this case, and for this reason it cannot be transformed into a contour far removed from all the singular points as for the monosized case. The numerical solution of the modified Orr–Sommerfeld equation requires very small steps of integration in a critical layer when any singular point approaches the real y-axis.

The break in $\omega(\alpha, R)$ arises when any singular point crosses the real y-axis, and hence the number of breaks equals the number of particle sizes. The α-dependence of $\mathrm{Im}(\omega)$ for dust containing particles of three sizes is presented in figure 21. One interval of α obtained for the monosized case (dashed-and-dotted lines) transforms into three intervals for polydisperse dust (solid lines) where two TS modes exist (figure 21*a*) or intervals where the eigenvalue problem has no solution (figure 21*b*). The individual interval of overlap or gap in $\mathrm{Im}(\omega)(\alpha)$ decreases with the number of sizes since the volume density of every size also decreases. However the total interval of overlap or gap in the $\mathrm{Im}(\omega)$ dependence on α remains finite. This conclusion follows also from the perturbation theory, which can be used when f is small, and for the discrete distribution (5.1) can be rewritten as

$$\omega = \omega_0 + f\sum_j F_j \omega_1(\gamma_j) + O(f^2) \quad \text{as} \quad f \ll 1.$$

A correction to the clean-gas eigenvalue ω_0 yielded by dust of size a_j°, $fF_j\omega_1(\gamma_j)$, is the discontinuous function along the curves l_j, which are governed by the equation (6.1) with γ replaced by γ_j. One interval of overlap or gap $\Delta\alpha$ transforms in the polydisperse case into a sequence of intervals $\Delta\alpha_j$ evaluated on l_j similar to (6.5): $\Delta\alpha_j = fF_j \mathrm{Im}\left[\omega_1(\gamma_j)\right] |\partial \mathrm{Im}\,\omega_0/\partial\alpha|^{-1} + O(f^2)$. As a result we have $\sum_j \Delta\alpha_j/\Delta\alpha \to \mathrm{const}$ as $f \to 0$.

It should be noted that the number of modes existing at the same α may be greater than two when the dust content is sufficiently large. So three modes of the TS wave are obtained for dust containing particles of two sizes (see figure 22).

https://doi.org/10.1017/S0022112098001256 Published online by Cambridge University Press

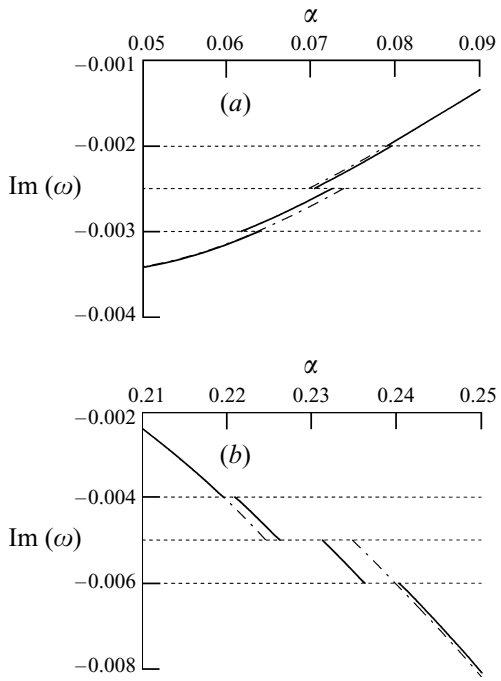


FIGURE 21. Discontinuity of the dependence of Im (ω) at $f = 0.04$, (*a*) $R = 500$ and (*b*) $R = 1000$ for dust containing particles of three sizes with $\gamma_1 = 4 \times 10^{-6}$, $\gamma_2 = 5 \times 10^{-6}$, $\gamma_3 = 6 \times 10^{-6}$, $F_1 = F_3 = 0.25$, $F_2 = 0.5$ (solid lines) in comparison with Im (ω) for the monosized case $\gamma = 5 \times 10^{-6}$ (dashed-and-dotted lines).

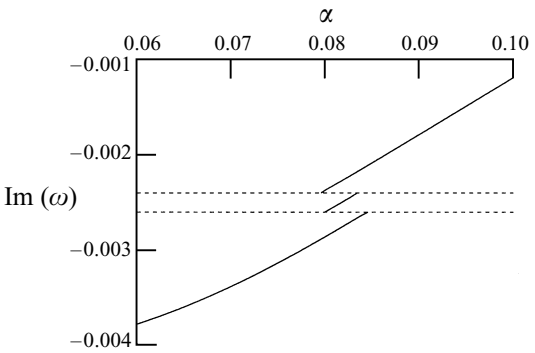


FIGURE 22. Discontinuity of the dependence of Im (ω) on α at $f = 0.1$, $R = 500$ for dust containing particles of two sizes with $\gamma_1 = 4.8 \times 10^{-6}$, $\gamma_2 = 5.2 \times 10^{-6}$, $F_1 = F_2 = 0.5$. There is an interval where three TS modes exist.

7.2. *Continuous distribution in* γ

When the number of particle sizes tends to infinity the discrete distribution F_j can be replaced by the continuous one, F, satisfying the normalization condition $\int F \mathrm{d}\gamma = 1$. For the unstable wave the eigenvalue problem is again governed by the modified Orr–Sommerfeld equation with $\widetilde{U}$ given by

$$\widetilde{U} = U + f\,(U - c) \int_0^\infty F\,(\gamma)\, \Lambda\,(y;\gamma)\, \mathrm{d}\gamma. \tag{7.1}$$

https://doi.org/10.1017/S0022112098001256 Published online by Cambridge University Press

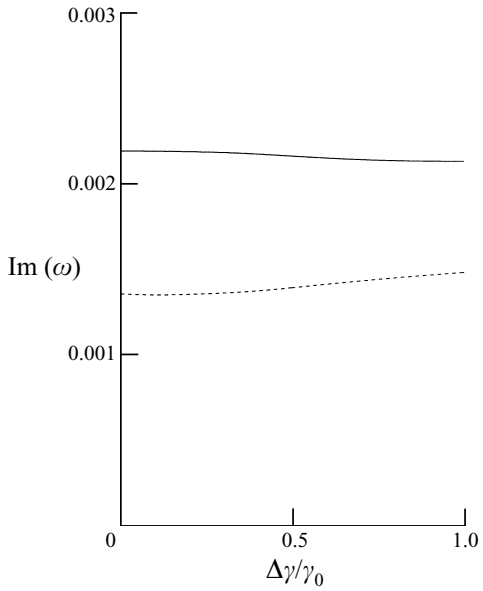


FIGURE 23. Growth rate for polydisperse dust as a function of the relative standard deviation at $R = 1000$, $f = 0.04$, $\gamma_0 = 10^{-3}$ (solid line) and $\gamma_0 = 10^{-4}$ (dashed line).

In this case the integral (7.1) is a regular function since the Λ dependence on γ has no singularity. Below we assume that F obeys the cut normal distribution

$$F = \left[\frac{\pi^{1/2}\Delta\gamma}{2}\mathrm{erfc}\left(-\frac{\gamma_0}{\Delta\gamma}\right)\right]^{-1}\exp\left[-\left(\frac{\gamma-\gamma_0}{\Delta\gamma}\right)^2\right], \quad 0 \leqslant \gamma < \infty. \tag{7.2}$$

The α dependence of the growth rate calculated for $\gamma_0 = 10^{-4}$, $\Delta\gamma = 0.5 \times 10^{-4}$ is shown in figure 20 by a solid line. It is close to that obtained for the discrete distribution in γ. In figure 23 $\mathrm{Im}(\omega)$ is shown as a function of relative standard deviation, $\Delta\gamma/\gamma_0$. For $\gamma_0 = 10^{-3}$ the growth rate decreases with $\Delta\gamma/\gamma_0$, and hence the damping effect is even greater than that for the monosized case $(\Delta\gamma/\gamma_0 = 0)$. However for $\gamma_0 = 10^{-4}$ the growth rate increases with $\Delta\gamma/\gamma_0$, and the polydisperse dust damps the instability wave to a smaller degree than the monosized dust. The reason is that the number of the particles with size close to the optimum value becomes smaller in this case.

The sequence of singular points $y_c(\gamma_j)$ obtained for the discrete distribution transforms into the singular line, $y_c(\gamma)$. For the stable wave, $\mathrm{Im}(\omega) < 0$, this line crosses the path of integration in (7.1). As a result $\widetilde{U}$ becomes a non-regular function of y. In order to illustrate this feature we estimate the integral sums corresponding to the integral in (7.1). To approximate (7.2) the discrete distribution

$$F_j = \frac{\exp\left[-\left(\dfrac{\gamma_j-\gamma_0}{\Delta\gamma}\right)^2\right]}{\displaystyle\sum_{j=1}^{\infty}\exp\left[-\left(\frac{\gamma_j-\gamma_0}{\Delta\gamma}\right)^2\right]} \tag{7.3}$$

https://doi.org/10.1017/S0022112098001256 Published online by Cambridge University Press

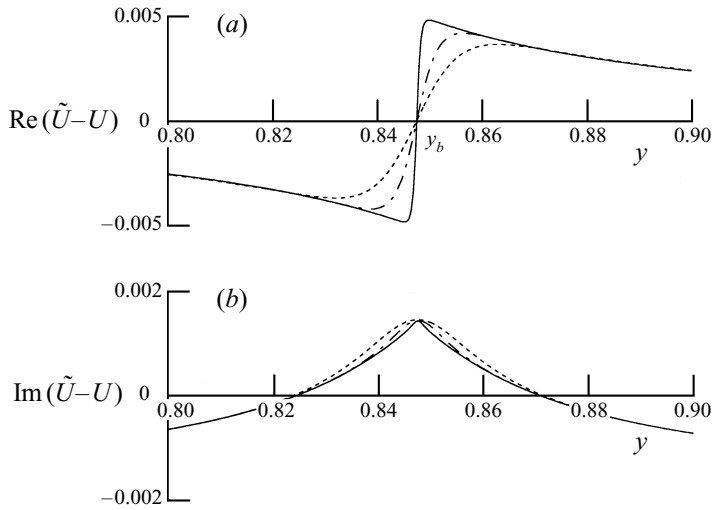


FIGURE 24. Profiles of $\widetilde{U}-U$ at $R=500$, $\alpha=0.07$, $\omega=0.02+\mathrm{i}\,0.0025$, $f=0.04$, $\gamma_0=5\times10^{-6}$, $\Delta\gamma=2.5\times10^{-6}$ for distribution (7.3) with $n=2$ (dashed lines), 4 (dashed-dotted lines) and 20 (solid lines). As n increases the profile tends to the limiting dependence corresponding to the continuous distribution (7.2). (*a*) The real part of this limiting profile has a break while (*b*) the imaginary part has a break in its derivative.

is used. Here

$$\gamma_j=\gamma_r+\frac{\Delta\gamma}{n}\left(j-\tfrac{1}{2}\right),$$

where n is some integer and γ_r is the remainder of the division of $\left(-\mathrm{Im}\,(\omega)/R\right)$ by $\Delta\gamma/n$. The profiles of $\widetilde{U}-U$ calculated for the discrete distributions (7.3) at $R=500$, $\alpha=0.07$, $\omega=0.02+\mathrm{i}\,0.0025$, $f=0.04$, $\gamma_0=5\times10^{-6}$, $\Delta\gamma=2.5\times10^{-6}$ and $n=2$, 4 and 20 are shown in figure 24. As n increases the profiles tend to the limiting dependence corresponding to the continuous distribution (7.2). It is seen that not only the limiting profile but also its derivative are discontinuous. The discontinuity of the integral in (7.1) is again due to the fact that its integrand has a pole, in this case in the complex γ-plane. The pole position is governed by the following equation:

$$\gamma_c(y)=-\frac{\mathrm{Im}\,(\omega)}{R}+\mathrm{i}\frac{\mathrm{Re}\,(\omega)-\alpha U(y)}{R}. \tag{7.4}$$

A break in $\widetilde{U}(y)$ arises when γ_c crosses the path of the integration in (7.1); γ_c is on the real axis at $y=y_b$ where y_b is given by $U(y_b)=\mathrm{Re}\,(c)$. It follows from (7.4) that $\mathrm{Re}\,(\gamma_c)>0$ for $\mathrm{Im}\,(\omega)<0$, and vice versa. Thus γ_c is on the path of the integration $[0,+\infty)$ only for the stable wave while for the unstable wave $\widetilde{U}(y)$ remains continuous.

Because of the discontinuity of the modified velocity profile its first and second derivatives should be treated as the singular generated functions at $\mathrm{Im}\,(\omega)<0$, so that

$$\left.\begin{aligned}\frac{\mathrm{d}\widetilde{U}}{\mathrm{d}y}&=\left\{\frac{\mathrm{d}\widetilde{U}}{\mathrm{d}y}\right\}+\left[\widetilde{U}\right]\delta(y-y_b),\\ \frac{\mathrm{d}^2\widetilde{U}}{\mathrm{d}y^2}&=\left\{\frac{\mathrm{d}^2\widetilde{U}}{\mathrm{d}y^2}\right\}+\left[\frac{\mathrm{d}\widetilde{U}}{\mathrm{d}y}\right]\delta(y-y_b)+\left[\widetilde{U}\right]\frac{\mathrm{d}\delta(y-y_b)}{\mathrm{d}y}.\end{aligned}\right\} \tag{7.5}$$

https://doi.org/10.1017/S0022112098001256 Published online by Cambridge University Press

Here $\{f\}$ denotes the piece-wise continuous function, δ is the Dirac delta function and

$$[f] = f(y_b + 0) - f(y_b - 0)$$

is the value of the break. An application of the integral Cauchy's theorem for the evaluation of the jump conditions for the modified velocity and its first derivative yields

$$\left[\widetilde{U}\right] = 2\pi f \frac{R}{\alpha} F(\gamma_b)\gamma_b^2, \quad \left[\frac{\mathrm{d}\widetilde{U}}{\mathrm{d}y}\right] = -2\pi \mathrm{i} f \frac{\mathrm{d}U}{\mathrm{d}y}(y_b)\frac{\mathrm{d}\left(F\gamma^2\right)}{\mathrm{d}\gamma}(\gamma_b), \tag{7.6}$$

where

$$\gamma_b = \gamma(y_b) = -\frac{\mathrm{Im}(\omega)}{R}.$$

The singular functions appearing in $\mathrm{d}^2\widetilde{U}/\mathrm{d}y^2$ (second and third terms in (7.5)) and hence in the modified Orr–Sommerfeld equation, result in the second and third derivatives of the eigenfunction being discontinuous at y_b, while φ and $\mathrm{d}\varphi/\mathrm{d}y$ remain continuous. In view of (7.5) the jump conditions for $\mathrm{Im}(\omega) < 0$ are

$$\left[\frac{\mathrm{d}^2\varphi}{\mathrm{d}y^2}\right] = -\mathrm{i}\alpha R\left[\widetilde{U}\right]\varphi(y_b), \quad \left[\frac{\mathrm{d}^3\varphi}{\mathrm{d}y^3}\right] = -\mathrm{i}\alpha R\left[\frac{\mathrm{d}\widetilde{U}}{\mathrm{d}y}\right]\varphi(y_b). \tag{7.7}$$

Thus the eigenfunction φ satisfies the regular Orr–Sommerfeld equation in the intervals $(0, y_b)$, (y_b, ∞) with functions $\widetilde{U}$, $\mathrm{d}^2\widetilde{U}/\mathrm{d}y^2$ being replaced by $\{\widetilde{U}\}$, $\{\mathrm{d}^2\widetilde{U}/\mathrm{d}y^2\}$ respectively. The boundary conditions are (2.10), (2.11) and the jump conditions (7.7).

The numerical procedure used to solve this boundary-value problem is similar to that described in § 4. The discontinuous dependence of the growth rate obtained for the monosized dust or for a discrete distribution in particle size transforms into a continuous one for a continuous distribution. This effect is illustrated in figure 25 where $\mathrm{Im}(\omega)$, calculated for F given by (7.2) and different standard deviations $\Delta\gamma$, is presented as a function of α. The solution also exists within the interval of the gap (see figure 25*b*). Within the overlap interval one more mode is added (see figure 25*a*). The solution obtained is a non-regular function of independent parameters. It may be treated as the limit of the piece-wise regular dependence corresponding to the discrete distribution (7.3) as $n \to \infty$. The number of breaks also tends to infinity with the width of every break tending to zero. The profiles of real and imaginary parts of the perturbed streamwise velocity calculated for $R = 1000$, $\alpha = 0.23$ $f = 0.04$, $\gamma_0 = 5 \times 10^{-6}$, $\Delta\gamma = 2 \times 10^{-7}$, $\omega = 0.0788 - \mathrm{i}\,0.0050$ are shown in figure 26. As predicted above, their derivatives are discontinuous at $y = y_b$.

Consider the limiting case $\Delta\gamma \to 0$ corresponding to near-monosized dust. Note, that $\Delta\gamma$ is assumed to be small but finite, while the amplitude of perturbations ϵ is asymptotically small, so that the linearization of the governing equations is still valid. The limiting dependence differs from that obtained in § 6. For $\mathrm{Im}(\omega) \neq -R\gamma_0$ it tends to the values corresponding to an accurately monosized case. Within the intervals of overlap or gap we have the additional solution tending to $\mathrm{Im}(\omega) = -R\gamma_0$.

The multi-mode regime does not occur for all standard deviation but only for small $\Delta\gamma$, when the number of particles with γ close to its resonant value is sufficiently large. For given $\Delta\gamma$ the required amount of such particles can be achieved by enhancing the dust content. In figure 27 $\mathrm{Im}(\omega)$ is shown for $R = 500$, $\gamma_0 = 5 \times 10^{-6}$, $\Delta\gamma/\gamma_0 = 0.02$ as a function of two independent variables α and f. Three modes of the TS wave exist when the dust content is greater than the critical value $f \approx 0.033$.

https://doi.org/10.1017/S0022112098001256 Published online by Cambridge University Press

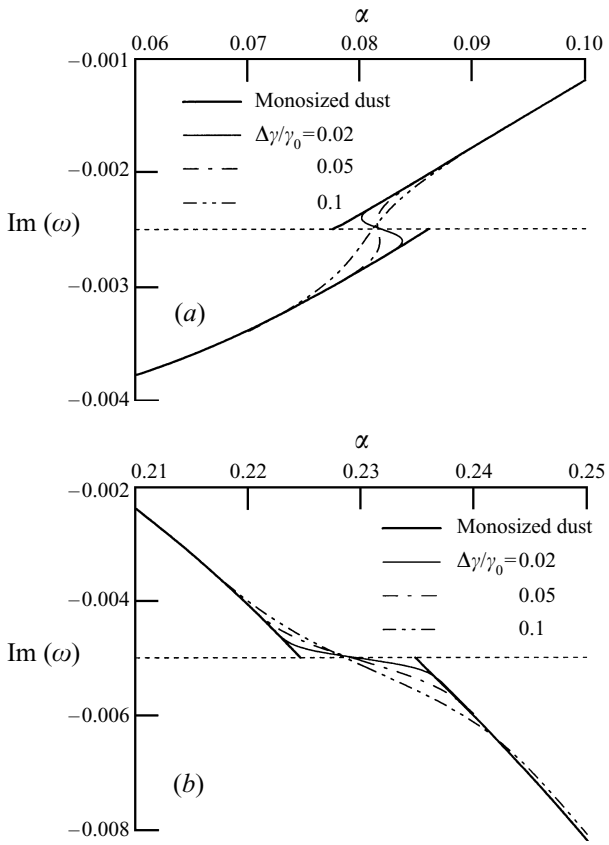


FIGURE 25. $\mathrm{Im}(\omega)$ vs. α for the continuous distribution F given by (7.2) at $\gamma_0 = 5 \times 10^{-6}$: (*a*) $R = 500$, $f = 0.1$ and (*b*) $R = 1000$, $f = 0.04$ and different standard deviations $\Delta\gamma$. The discontinuous dependence obtained for monosized dust or for a discrete distribution in particle size transforms into a continuous one. For case (*a*) one or three modes may exist depending on $\Delta\gamma/\gamma_0$.

At small f the eigenvalue can be evaluated for the continuous distribution in γ within the framework of perturbation theory in two ways. One can present the linear perturbation as a superposition of the perturbations resulting from every size of particle:

$$\omega = \omega_0 + f \int_0^\infty F(\gamma)\, \omega_1(\gamma)\, \mathrm{d}\gamma + O\left(f^2\right). \tag{7.8}$$

On the other hand, the eigenvalue perturbation can be calculated directly from equations (5.1), (5.4). In this case U_1, entering in operator L_{U_1} in (5.4), should be replaced by the integral over γ, so that

$$U_1 = \frac{y}{2}\frac{\mathrm{d}U_0}{\mathrm{d}y} + (U_0 - c_0) \int_0^\infty F(\gamma)\, \Lambda_0(y;\gamma)\, \mathrm{d}\gamma.$$

For the unstable TS wave ($\mathrm{Im}(\omega_0) > 0$), the equivalence of these two methods of eigenvalue calculation is evident since they differ by the order of integration over y and γ.

https://doi.org/10.1017/S0022112098001256 Published online by Cambridge University Press

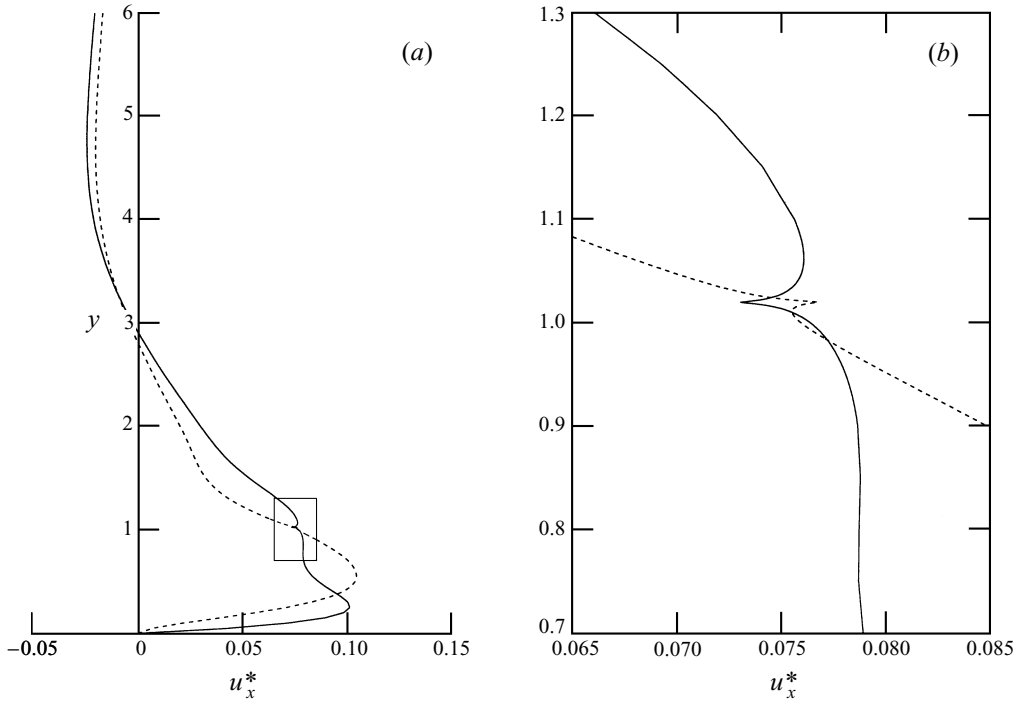


FIGURE 26. Profiles of real (solid lines) and imaginary (dashed lines) parts of the perturbed streamwise velocity for the continuous distribution in particle size at $R = 1000$, $\alpha = 0.23$, $f = 0.04$, $\gamma_0 = 5 \times 10^{-6}$, $\Delta\gamma = 2 \times 10^{-7}$, $\omega = 0.0788 - \mathrm{i}\,0.0050$. (*b*) Expanded view of the boxed region in (*a*).

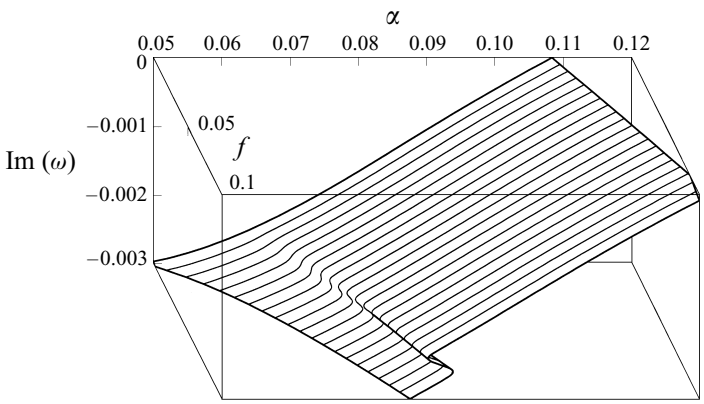


FIGURE 27. $\mathrm{Im}\,(\omega)$ calculated at $R = 500$, $\gamma_0 = 5 \cdot 10^{-6}$, $\Delta\gamma/\gamma_0 = 0.02$ as a function of α, f. Three modes of the TS wave exist when the dust content is greater than the critical value $f \approx 0.033$.

For the second approach to be valid for the stable TS wave ($\mathrm{Im}\,(\omega_0) < 0$), U_1 should be treated as a singular generated function, so that

$$\frac{\mathrm{d}^2 U_1}{\mathrm{d}y^2} = \left\{\frac{\mathrm{d}^2 U_1}{\mathrm{d}y^2}\right\} + \left[\frac{\mathrm{d}U_1}{\mathrm{d}y}\right] \delta\,(y - y_{b0}) + [U_1]\,\frac{\mathrm{d}\delta\,(y - y_{b0})}{\mathrm{d}y}.$$

Here y_{b0} is governed by the equation $U\,(y_{b0}) = \mathrm{Re}\,(c_0)$. As a result we have for the

https://doi.org/10.1017/S0022112098001256 Published online by Cambridge University Press

eigenvalue at small f:

$$\omega = \omega_0 - f\frac{\left(\varphi_0^+, \mathrm{L}_{\{U_1\}}\varphi_0\right) + \Psi\,(y_{b0})}{\left(\varphi_0^+, \mathrm{L}_\omega\varphi_0\right)} + O(f^2), \tag{7.9}$$

where

$$\Psi = -\left[\frac{\mathrm{d}U_1}{\mathrm{d}y}\right]\overline{\varphi_0^+}\varphi_0 + [U_1]\frac{\mathrm{d}\left(\overline{\varphi_0^+}\varphi_0\right)}{\mathrm{d}y}.$$

Evaluating $[U_1]$ and $\left[\mathrm{d}U_1/\mathrm{d}y\right]$ similarly to (7.6) one can obtain

$$\Psi = 2\pi\left[\frac{R}{\alpha}F\,(\gamma_{b0})\,\gamma_{b0}^2\frac{\mathrm{d}\left(\overline{\varphi_0^+}\varphi_0\right)}{\mathrm{d}y} + \mathrm{i}\frac{\mathrm{d}U_0}{\mathrm{d}y}\frac{\mathrm{d}\left(F\gamma^2\right)}{\mathrm{d}\gamma}\,(\gamma_{b0})\,\overline{\varphi_0^+}\varphi_0\right],$$

where $\gamma_{b0} = -\mathrm{Im}\,(\omega_0)/R$.

It follows from (7.9) that ω_1, being the superposition of the discontinuous functions $\omega_1\,(\gamma)$ (see equations (7.8) and (6.2)) in the region $\mathrm{Im}\,(\omega_0) < 0$, is, nevertheless, a continuous function of α, R.

8. The effect of the lift force

The present investigation is carried out on the assumption that the dust is under the action of the Stokes drag only. However, particles moving in a shear flow experience a lift force due to the combination of the slip velocity and the shear. The force on a single particle is given by (Saffman 1965)

$$F_{Sa}^\circ = c\rho^\circ a^{\circ 2}\left(U_x^\circ - V_x^\circ\right)\left(\nu^\circ\frac{\partial U_x^\circ}{\partial y^\circ}\right)^{1/2}.$$

A maximum value of the lift force coefficient, c, which depends on the relation between the two particle Reynolds numbers based on the slip velocity and on fluid shear is $c\,(0) = 6.46$ (Saffman 1965).

For the governing equations (2.4), (2.5) to be valid, the unsteady lift force due to the perturbation of the streamwise slip velocity must be much less than the unsteady normal Stokes drag. This requirement is equivalent to the following inequality:

$$\frac{c}{6\pi}a^\circ\frac{u_x^\circ - v_x^\circ}{u_y^\circ - v_y^\circ}\left(\frac{1}{\nu^\circ}\frac{\partial U_x^\circ}{\partial y^\circ}\right)^{1/2} \ll 1,$$

or in dimensionless form:

$$\frac{c}{2\sqrt{2}\pi}\frac{u_x^* - v_x^*}{u_y^* - v_y^*}\left(\frac{1}{R\gamma\rho_p}\frac{\partial U}{\partial y}\right)^{1/2} \ll 1. \tag{8.1}$$

In view of (2.6) the ratio of slip velocities in (8.1) can be expressed as

$$\frac{u_x^* - v_x^*}{u_y^* - v_y^*} = \frac{u_x^*}{u_y^*} - \mathrm{i}\frac{\partial U}{\partial y}\frac{\Lambda}{\alpha U - \omega}. \tag{8.2}$$

Taking the characteristic values of the first term in (8.2) $u_x^*/u_y^* = 2$ (see figures 7, 8), $\alpha = 0.1$, $U = 1$, $\partial U/\partial y = 0.3$, $\Lambda = 1$, one can see that the first and the second terms in the right-hand side of (8.2) are of the same order in the major portion of

https://doi.org/10.1017/S0022112098001256 Published online by Cambridge University Press

the boundary layer. As a result the ratio (8.2) can be estimated as 3. However, in a critical layer the denominator of the second term is of the order of $\mathrm{Im}\,(\omega)$. The characteristic value of the growth rate, 0.001, is one hundred times less than that of α. Hence, the ratio of the slip velocities can be estimated in a critical layer as 300.

Inequality (8.1) is fulfilled over the entire boundary layer only for very large γ, i.e. for very small particles. For the regime of most efficient damping of the instability wave the ratio of two normal forces is not small in a critical layer. So at $R = 1000$, $\gamma = 10^{-4}$, $\rho_p = 800$ the ratio can be estimated as 10 in the critical layer and 0.1 in the remainder of the boundary layer. Such values of γ, ρ_p correspond, for example, at standard conditions to the dusty-gas flow composed of air and water droplets of radius $a^\circ = 10^{-6}$ m with upstream velocity $U^\circ_\infty = 100$ m s^{-1}.

Thus the unsteady lift force may be neglected in comparison with the normal Stokes drag in the major portion of the boundary layer, but in a critical layer such neglect is not justified. Though this region is small, its influence on the dissipation of the disturbance energy may be most significant. It would be expected that the presence of particles just in a critical layer results in reduction in growth rate. Hence the role of the lift force in the unsteady momentum transfer requires special consideration. It may be clarified by solution of the linear stability problem for the flow with the non-uniform distribution of particle density and taking the account of all the mechanisms of momentum transfer.

The governing equations are derived for a boundary-layer flow under one more assumption that the dust mean-flow velocity resembles closely that of the gas, and its density equals the free-stream value. This requires the relaxation length of the mean-flow particle velocity to be small compared with the distance X° from the leading edge of the plate. As the particles experience two forces in a boundary layer, Stokes drag and lift, the dust flow has two relaxation lengths, L°_{St} given by (1.1) and L°_{Sa}. These two length scales correspond to the relaxation of streamwise and normal velocities. For the boundary-layer flow over a flat plate L°_{Sa} was introduced as (Asmolov 1992)

$$L^\circ_{Sa} = \frac{1}{81}\left[\frac{c\,(0)}{\pi}\right]^{4/3}\left[\frac{\partial U_0}{\partial y}\,(0)\right]^2 \left(U^\circ_\infty/\mu^\circ\right)^3 a^{\circ 4}\rho^{\circ 5/3}\rho_p^{\circ 4/3},$$

where μ° is the dynamic viscosity of the gas and $(\partial U_0/\partial y)/\,(0) = 0.332$. The above assumption remains valid when

$$L^\circ_{St}/X^\circ \ll 1, \quad L^\circ_{Sa}/X^\circ \ll 1,$$

or in dimensionless form, respectively,

$$\gamma^{-1}R^{-2} \ll 1, \tag{8.3}$$

$$\frac{1}{4}\left[\frac{c\,(0)}{\pi}\right]^{4/3}\left[\frac{\partial U_0}{\partial y}\,(0)\right]^2 \rho_p^{-2/3}\gamma^{-2}R^{-2} \ll 1. \tag{8.4}$$

That inequalities are satisfied when the particles are sufficiently small. At $R = 1000$, $\gamma = 10^{-4}$, $\rho_p = 800$ the ratios L°_{St}/X°, L°_{Sa}/X° can be estimated as 0.01 and 0.08 respectively. As L°_{Sa} is proportional to $a^{\circ 4}$ (or, equivalently, to γ^{-2}) and L°_{St} to $a^{\circ 2}$ (or, equivalently, to γ^{-1}), (8.4) may cease to be true with increasing particle size while the inequality (8.3) remains valid. For example, at $\gamma = 2\times 10^{-5}$ and the other dimensionless parameters the same we have $L^\circ_{St}/X^\circ \approx 0.05$, $L^\circ_{Sa}/X^\circ \approx 2$. This corresponds to water droplets of radius $a^\circ = 2\times 10^{-6}$ m.

Therefore, L°_{St} is usually small compared with X°, but the relaxation length of the normal velocity, L°_{Sa}, may be of the order of X°, even for not-too-large particles.

https://doi.org/10.1017/S0022112098001256 Published online by Cambridge University Press

As a result the particle density distribution in the region under investigation is non-homogeneous, and the mean-velocity profile ceases to obey the Blasius solution. Summarizing, it may be concluded that the lift force in both steady and unsteady momentum transfer should be taken into account when investigating the linear stability of dusty-gas flow containing large particles.

9. Conclusions

The linear stability of dusty-gas flow in a boundary layer over a flat plate has been considered. The equations for the disturbances of gas and dust flows are reduced to a modified Orr–Sommerfeld equation similar to that obtained by Saffman (1962) for plane parallel flows. The dust effect on the monochromatic Tollmien–Schlichting wave has been investigated for both mono- and polydisperse particles.

Two limiting cases of coarse and fine particles have been studied. The addition of fine dust enhances the critical Reynolds number while coarse dust reduces it. Qualitatively the effect is the same as for the case of plane parallel flows (Saffman 1962) when the particles modify only the disturbance flow, but do not influence the mean flow. However, the stability characteristics are expressed in terms of those for a clean gas in some other way, because of the modification of the mean boundary-layer flow.

The eigenvalue problem has been solved by a direct integration using the orthonormalization method. Also, a perturbation method has been developed for small particle mass content. The calculations based on both approaches show that unsteady momentum exchange between phases due to the viscous drag force results in significant reduction in the growth rate of the unstable TS wave. The most efficient suppression takes place for the intermediate particle size when the relaxation length of the particle velocity is close to the wavelength of the wave. The dust effect in this case is many times greater than for either coarse or fine particles.

For the steady TS wave a discontinuity of the eigenvalue due to resonant acceleration of the monosized particles in a critical layer is observed. As a result a domain in the space of independent parameters – Reynolds number R, wavenumber α – arises where two discrete TS modes exist and a domain where no TS mode may exist.

The analysis developed for the monosized dust has been extended to the flow containing particles of different sizes. The damping effect of the polydisperse dust is similar to the monosized case. For a damped wave and discrete distribution in particle radii the number of discontinuities in $\omega(\alpha, R)$ equals the number of particle sizes. For the continuous distribution $\omega(\alpha, R)$ is a continuous but non-regular function. The eigenfunction becomes a non-smooth function of the normal coordinate in this case.

The possible effect of a lift force, which has been neglected in the present study for both mean and disturbance flow, is discussed. The unsteady lift may be ignored in comparison with the normal Stokes drag in the major portion of the boundary layer, but not in a critical layer. Lift should be also taken into account in the equations governing the mean dusty-gas flow when the particles are large ($a^\circ = 2 \times 10^{-6}$ m or larger at normal conditions and the upstream velocity $U_\infty^\circ = 100$ m s^{-1}).

The research was supported by International Science and Technology Center (ISTC) under Project No. 199 and Russian Foundation for Fundamental Research (Grants No. 95-01-01201a and No. 96-01-01245). Helpful comments from the referees were gratefully appreciated.

https://doi.org/10.1017/S0022112098001256 Published online by Cambridge University Press

REFERENCES

Asmolov, E. S. 1992 Motion of a suspension in the laminar boundary layer on a flat plate. *Fluid Dyn.* **27**, 49–54.

Asmolov, E. S. & Manuilovich, S. V. 1994 Stability of two-phase boundary layer on a flat plate. In *Laminar-Turbulent Transition. IUTAM Symp., Senday/Japan. September 5-9, 1994,* pp. 333–340. Springer.

Asmolov, E. S. & Manuilovich, S. V. 1995 Stability of dusty-gas laminar boundary layer. In *IUTAM Symp. on Nonlinear Instability and Transition in 3D Boundary Layer, Manchester, UK, Abstracts.*

Godunov, S. K. 1961 On the numerical solution of the boundary-value problem for the system of linear ordinary differential equations. *Usp. Mat. Nauk* **16**, No. 3, 171–174 (in Russian).

Lin, C. C. 1955 *The Theory of Hydrodynanic Stability.* Cambridge University Press.

Marble, F. E. 1962 Dynamics of a gas containing small solid particles. In *Proc. 5th AGARD Colloq. on Combustion and Propulsion, Braunschweig,* pp. 175–213. Pergamon.

Marble, F. E. 1970 Dynamics of dusty gases. *Ann. Rev. Fluid Mech.* **2**, 397–446.

Michael, D. H. 1964 The stability of plane Poiseuille flow of a dusty gas. *J. Fluid Mech.* **18**, 19–32.

Osiptsov, A. N. 1980 Structure of the laminar boundary layer of a disperse medium on a flat plate. *Fluid Dyn.* **23**, 80–87.

Saffman, P. G. 1962 On the stability of laminar flow of a dusty gas. *J. Fluid Mech.* **13**, 120–128.

Saffman, P. G. 1965 The lift on a small sphere in a slow shear flow. *J. Fluid Mech.* **22**, 385–400; and Corrigendum. *J. Fluid Mech.* **31**, 1968, 624.

Schlichting, H. 1968 *Boundary Layer Theory.* McGraw-Hill.

Shaqfeh, E. S. G. & Acrivos, A. 1987 The effects of inertia on the stability of the convective flow in inclined particle settlers. *Phys. Fluids* **30**, 960–973.

Yang Yongqi, Chung, J. N., Troutt, T. R. & Crowe C. T. 1990 The influence of particles on the spatial stability of two-phase mixing layers. *Phys. Fluids* A **2**, 1839–1845.

Zhang, K., Acrivos, A. & Schaflinger, U. 1992 Stability in a two-dimensional Hagen-Poiseuille resuspension flow. *Intl J. Multiphase Flow* **18**, 51–63.

https://doi.org/10.1017/S0022112098001256 Published online by Cambridge University Press